Author Manuscript

Author Manuscript

Author Manuscript

Author Manuscript

HHS Public Access

Author manuscript

Neuron. Author manuscript; available in PMC 2019 September 19.

Published in final edited form as:

Neuron. 2018 September 19; 99(6): 1274–1288.e6. doi:10.1016/j.neuron.2018.08.044.

Kappa Opioid Receptor Distribution and Function in Primary Afferents

Lindsey M. Snyder[1], **Michael C. Chiang**[1], **Emanuel Loeza-Alcocer**[1], **Yu Omori**[1], **Junichi Hachisuka**[1], **Tayler D. Sheahan**[1], **Jenna R. Gale**[1], **Peter C. Adelman**[1], **Elizabeth I. Sypek**[2], **Stephanie A. Fulton**[1], **Robert L. Friedman**[1], **Margaret C. Wright**[1], **Melissa Giraldo Duque**[1], **Yeon Sun Lee**[3], **Zeyu Hu**[1], **Huizhen Huang**[1,4], **Xiaoyun Cai**[1], **Kimberly A. Meerschaert**[1], **Vidhya Nagarajan**[1], **Toshiro Hirai**[5], **Gregory Scherrer**[2,6], **Daniel H. Kaplan**[5], **Frank Porreca**[7], **Brian M. Davis**[1], **Michael S. Gold**[1], **H. Richard Koerber**[1], and **Sarah E. Ross**[1,8]

[1]Department of Neurobiology and the Pittsburgh Center for Pain Research, University of Pittsburgh, Pittsburgh, PA 15213, USA

[2]Department of Anesthesiology, Perioperative and Pain Medicine, Department of Molecular and Cellular Physiology, Department of Neurosurgery, Stanford Neurosciences Institute Stanford University, Stanford, CA 94305, USA

[3]Department of Chemistry and Biochemistry, University of Arizona, Tucson, AZ 85721, USA

[4]Tsinghua University School of Medicine Beijing, China

[5]Departments of Dermatology and Immunology, University of Pittsburgh, Pittsburgh, PA 15213, USA

[6]New York Stem Cell Foundation — Robertson Investigator, Stanford University, Palo Alto, CA 94304, USA

[7]Department of Pharmacology, University of Arizona, Tucson, AZ 85719, USA

[8]Department of Anesthesiology, University of Pittsburgh, Pittsburgh, PA 15213, USA

SUMMARY

Primary afferents are known to be inhibited by kappa opioid receptor (KOR) signaling. However, the specific types of somatosensory neurons that express KOR remain unclear. Here, using a newly

Corresponding Authors: Michael S. Gold, W1451 Biomedical Science Tower, 200 Lothrop St., Pittsburgh, PA 15213, msg22@pitt.edu. H. Richard Koerber, W1447 Biomedical Science Tower, 200 Lothrop St., Pittsburgh, PA 15213, rkoerber@pitt.edu. Sarah E. Ross, W1456 Biomedical Science Tower, 200 Lothrop St., Pittsburgh, PA 15213, saross@pitt.edu.
Lead Contact: Sarah E. Ross

AUTHOR CONTRIBUTIONS

Conceptualization - L.M.S., M.C.C., Y.O., J.H., P.C.A., S.E.R., G.S., M.S.G., H.R.K.
Methodology - Y.O., J.H., E.L.A.
Investigation - L.M.S., M.C.C., E.L.A., T.D.S, J.R.G., V.N., T.H., K.A.M., Y.O., J.H., P.C.A., E.I.S., S.F., R.L.F., M.G.D., M.W., Z.H., H.H., X.C., K.A.M., B.M.D.,
Writing – Original Draft - L.M.S. and S.E.R.
Writing – Review and Editing – L.M.S., S.E.R, M.S.G, H.R.K, and F.P.
Funding Acquisition - L.M.S., S.E.R., G.S., M.S.G., H.R.K., F.P., D.H.K., B.M.D.
Resources – Y.L., F.P.

CONFLICTS OF INTEREST

None of the authors has a conflict of interest.

Author Manuscript Author Manuscript Author Manuscript Author Manuscript

developed *KOR-cre* knockin allele, viral tracing, single-cell RT-PCR, and *ex vivo* recordings, we show that KOR is expressed in several populations of primary afferents: a subset of peptidergic sensory neurons, as well as low-threshold mechanoreceptors that form lanceolate or circumferential endings around hair follicles. We find that KOR acts centrally to inhibit excitatory neurotransmission from *KOR-cre* afferents in laminae I and III, and this effect is likely due to KOR-mediated inhibition of Ca^{2+} influx, which we observed in sensory neurons from both mouse and human. In the periphery, KOR signaling inhibits neurogenic inflammation, nociceptor sensitization by inflammatory mediators, and pain and itch behaviors. These experiments provide a rationale for the therapeutic use of peripherally restricted KOR agonists.

eTOC BLURB

Snyder et al. identify primary afferents that express the kappa opioid receptor in mouse and human and show that kappa opioid receptor signaling inhibits these cells in physiological and behavioral experiments.

Keywords

Pain; itch; somatosensation; Kappa Opioid Receptor; Oprk1; primary afferents; DRG; dorsal root ganglia; sensory neurons; dynorphin; nalfurafine; ICI204; 488; FE200665; mouse; human

INTRODUCTION

Opioids are known to modulate somatosensation and have been the focus of decades of research aimed at developing better treatments for pain. This class of molecules and their receptors comprise several primary subtypes including mu, delta, and kappa (Kieffer and Gaveriaux-Ruff, 2002). Mu opioid receptor (MOR) agonists, such as morphine, remain among the most widely used treatments for various acute and chronic pain conditions (Smith and Peppin, 2014). While often effective at relieving pain, MOR agonists are frequently accompanied by deleterious side effects such as respiratory depression and sedation (Boom et al., 2012), nausea and constipation (Porreca and Ossipov, 2009), and the development of tolerance (Bailey and Connor, 2005). In addition, millions of American have been estimated to suffer from substance abuse stemming from MOR agonist-based prescription pain relievers (Smith, 2017). As a result, the clinical potential of other classes of opioids have been the topic of great interest.

An appealing therapeutic target is the kappa opioid receptor (KOR). KOR is an inhibitory G-protein coupled receptor that is activated by the endogenous ligand dynorphin (Chavkin et al., 1982). KOR agonists reduce pain and itch (Cowan et al., 2015; Millan, 1990; Vanderah, 2010); however, KOR signaling plays many other roles across the nervous system. For instance, KOR signaling mediates negative emotional states including aversion, depressive-like behaviors, and drug reinstatement (Lalanne et al., 2014; Shippenberg et al., 2007). In addition, the naturally occurring KOR agonist salvinorin A, derived from Salvia divinorum, is a psychoactive drug that is taken recreationally (Chavkin et al., 2004; Sheffler and Roth, 2003). Thus, while KOR agonists could provide analgesic benefit, they nevertheless have limiting side effects and abuse liability.

Author Manuscript Author Manuscript Author Manuscript Author Manuscript

Given the problems associated with the activation of KOR in the CNS, targeting receptors in the periphery has emerged as an attractive strategy. KOR has been reported to be expressed by small, medium, and large diameter neurons in rat dorsal root ganglia (DRG) (Ji et al., 1995; Maekawa et al., 1994), but the specific types of sensory neurons that express KOR are unknown. In an effort to understand the therapeutic potential of peripherally restricted KOR agonists, we sought to identify which primary afferents express KOR and how activation of KOR on these cells modulates somatosensation.

RESULTS

KOR-cre knockin mouse as a tool to identify peripheral sensory neurons expressing KOR

A subpopulation of primary afferents in the mouse is known to respond to KOR agonists (Macdonald and Werz, 1986; Werz and Macdonald, 1984), but this subpopulation has not been characterized. We therefore generated a *KOR-cre* knockin allele in which Cre recombinase (Cre) replaces the initial coding sequence of the *Oprk1* gene (Cai et al., 2016). To validate that the *KOR-cre* allele mediates recombination in primary afferents that express *Oprk1,* we performed dual fluorescent *in-situ* hybridization (FISH) for *Oprk1* and *tdTomato* mRNA in mice that had received intrathecal administration of a Cre-dependent virus (AAV.FLEX.ChR2-tdTomato) (Dayton et al., 2012; Vulchanova et al., 2010). The vast majority of the primary afferents that expressed *tdTomato* mRNA also expressed *Oprk1* message and, conversely, most *Oprk1*-expressing afferents showed *tdTomato* mRNA expression (Figures 1A and 1B). To confirm these findings, we performed single-cell RT-PCR on virally-labeled *KOR-cre* primary afferents (AAV.FLEX.ChR2-tdTomato delivered IT). We found that most (10 of 12) *KOR-cre*-expressing neurons showed *Oprk1* expression by RT-PCR (Figure 1C). In contrast, in primary afferents that were not genetically labeled by the *KOR-cre* allele, *Oprk1* mRNA was not detected (Figure 1C). These findings suggest that the recombination mediated by the *KOR-cre* allele faithfully recapitulates the endogenous expression of *Oprk1.*

KOR is expressed in distinct neurochemical and anatomical subsets of primary afferents

We noted that primary afferents with both large and small diameter somata were labeled with the *KOR-cre* allele, suggesting that KOR is expressed in more than one type of sensory neuron. To address this possibility, we characterized *KOR-cre* neurons that were visualized using a Cre-dependent ChR2-tdTomato virus delivered IT (Dayton et al., 2012). In quadruple-labeling experiments, we found that almost all *KOR-cre* afferents were labeled with a small subset of markers: calcitonin gene-related peptide (CGRP), which marks peptidergic cells (Figures 2A and 2D) (Basbaum, 2008), Neurofilament-200 (NF200), which marks myelinated Aδ and Aβ fibers (Figures 2B and 2D) (Basbaum, 2008; Li et al., 2011), and tyrosine hydroxylase (TH), which marks a subset of C-fibers that includes low-threshold mechanoreceptors (Figures 2C and 2D) (Li et al., 2011; Seal et al., 2009). This pattern of co-labeling suggested that ~2/3 of *KOR-cre*-labeled sensory neurons are nociceptive (i.e., expressed CGRP (or CGRP and NF200)), whereas ~1/3 of *KOR-cre*-labeled neurons are low-threshold mechanoreceptors (LTMRs) (i.e., afferents expressed TH or NF200, but not CGRP (Le Pichon and Chesler, 2014)). Together, these three markers labeled 95% of the *KOR-cre* population (Figure 2D). In contrast, we observed little or no overlap of *KOR-cre*

Author Manuscript Author Manuscript Author Manuscript Author Manuscript

afferents with TRPM8-immunoreactive (IR) or parvalbumin-IR neurons, suggesting that *KOR-cre* does not cause recombination in either cool-sensing neurons (McKemy et al., 2002; Peier et al., 2002) or in proprioceptors (de Nooij et al., 2013) (Figures S1 and S2).

Since we and others have shown that KOR agonists inhibit itch (Cowan et al., 2015; Kardon et al., 2014), we were interested in determining whether itch responsive afferents, including somatostatin- (SST) and MrgprA3-expressing populations, express KOR. However, in these two populations we found limited overlap with *KOR-cre*-labeled neurons or *Oprk1* mRNA (Figures S1C – S1F). In experiments to assess the presence of KOR-expressing primary afferent terminals in the skin, we noted the recombination of some dermal cells (Figure S1G) that turned were subsequently identified as macrophages upon further characterization by flow cytometry (Figure S1H). However, we were unable to detect *Oprk1* mRNA in these cells, either by RT-PCR or fluorescence in situ hybridization, possibly due to a very low abundance of message or transient expression of *Oprk1* in these cells.

Many genes show a developmental pattern of expression that differs from that observed in adulthood. We therefore compared the recombination pattern that was observed when the reporter was introduced at different stages of development. In general, similar subsets of afferents were labeled (Figures S2A and S2B). However, *KOR-cre*-labeled sensory neurons that were marked when adult mice were infected with Cre-dependent viruses made up a smaller and more restricted population than that observed when the recombination occurred during embryonic or early post-natal development (Figure S2).

Since the *KOR-cre* allele appeared to mediate recombination in several populations of primary afferents, we next addressed whether these fibers terminate in distinct laminae of the spinal cord. To selectively visualize the central terminals of *KOR-cre*-expressing primary afferents (rather than *KOR-cre* spinal interneurons), Cre-dependent AAV viruses were either injected into the sciatic nerve of adult mice (Figures 2E, 2F and 2G), or delivered IP at P1 (Figures S3A and S3B). We observed that many *KOR-cre* afferents terminated in the superficial dorsal horn, where they co-localized with CGRP. In addition, we found *KOR-cre* afferents that terminated in laminae III-IV, the LTMR recipient zone. At least some of these fibers appeared to send collaterals in the dorsal funiculus (Figure S3A), consistent with the possibility that *KOR-cre* afferents include LTMRs that target the dorsal column nuclei (Horch et al., 1976). Taken together, the neurochemical and anatomical data support the idea that KOR is expressed by nociceptive peptidergic afferents that target lamina I, and presumed LTMRs that target laminae III-IV and the dorsal column nuclei.

KOR is expressed in lanceolate and circumferential low-threshold mechanoreceptors

The finding that *KOR-cre* mediates the recombination of afferents that target the LTMR-recipient zone in the deep dorsal horn was somewhat unexpected as there had been no previous studies that implicated KOR signaling in low-threshold mechanosensation. To investigate the identity of these afferent fibers further, we visualized their peripheral endings using Cre-dependent expression of ChR2-tdTomato. In the hairy skin of the hindpaw, we observed that *KOR-cre* labeled afferents formed lanceolate (Figure 3A) or circumferential (Figure 3B) endings around hair follicles. Many of these afferents co-expressed NF-200, indicating that they are myelinated, but they did not express CGRP. *KOR-cre* afferents with

Author Manuscript Author Manuscript Author Manuscript Author Manuscript

lanceolate or circumferential endings were also observed in the hairy back skin, where they targeted multiple hair follicle types (Figures S4A and S4B). This suggests that KOR is expressed by a subset of LTMRs that target hair follicles across the body. In contrast, *KOR-cre* afferents did not include afferents targeting Merkel disks or Meissner corpuscles in glabrous skin (data not shown).

To characterize the physiology of low-threshold *KOR-cre* afferents, we used the *ex vivo* skin-nerve preparation and teased fiber recordings (McIlwrath et al., 2007; Woodbury et al., 2001). ChR2-expressing *KOR-cre* afferents were identified through optogenetic tagging (Figures S5A and S5B) and then characterized by their responses to the application of constant mechanical force (1 – 100 mN). Using this approach, we observed cells with two distinct firing patterns in response to mechanical stimulation. The first responded to low-threshold stimulation (e.g., 5 or 10 mN) and consistently fired only once (at stimulus onset) or twice (at stimulus onset and offset) in response to mechanical stimulation throughout the range of forces tested (Figures 3C, S5C and S5E). This stimulus-response pattern is consistent with our anatomical data suggesting that *KOR-cre* afferents include rapidly adapting lanceolate fibers (Koerber and Woodbury, 2002; Li et al., 2011). A second type of *KOR-cre* afferent also responded to low-threshold stimulation (Figures 3D, S5D and S5E). However, these afferents fired throughout the period of mechanical stimulation, showing dramatically increased firing rates in response to increasing forces. These response properties (low-threshold but responsive across a large dynamic range) are also consistent with our anatomical data revealing afferents that form circumferential endings around hair follicles (Bai et al., 2015). Taken together, these functional data suggest KOR is present in at least three sensory neuron subtypes, including two that target hair follicles.

KOR is expressed by a transcriptionally distinct subset of peptidergic afferents

The majority of sensory neurons targeted by the *KOR-cre* allele were not LTMRs, but rather peptidergic (presumably nociceptive) afferents. We found that many of these *KOR-cre* afferents formed free nerve endings in the skin (Figure 4A), but they were not specific to the skin, as they were found in numerous other tissues. To characterize the peptidergic *KOR-cre* afferents further, we performed immunolabeling and found that two-thirds of *KOR-cre* afferents expressed CGRP, and half expressed substance P and/or TRPV1 (Figures 4B and 4C). Although most *KOR-cre* afferents expressed CGRP, it is important to note that there were many CGRP-positive afferents that did not show *KOR-cre* mediated recombination (e.g., Figure 4B, arrowheads). This observation led us to ask whether peptidergic neurons that express KOR are in some way distinct from peptidergic neurons that do not express KOR. To investigate this question, we used single-cell quantitative RT-PCR, restricting analysis to afferents that expressed Calcα (which encodes CGRP). Within this peptidergic category, 15 *KOR-cre* positive afferents in which the presence of *Oprk1* message was subsequently confirmed were compared to 20 *KOR-cre* negative neurons (Figure 4D). This analysis revealed a number of markers for peptidergic neurons — *Calcα, Tac1, Trpv1, Gfrα3* and *Ptgir* — that were expressed at significantly higher levels in *Oprk1*-positive relative to *Oprk1*-negative neurons (Figures 4E – 4J). These findings suggest that, within the peptidergic class of primary afferents, KOR is preferentially expressed in a transcriptionally distinct subset of neurons.

Author Manuscript Author Manuscript Author Manuscript Author Manuscript

The finding that *Oprk1* is detected in a transcriptionally distinct subset of peptidergic afferents raised the possibility that *Oprk1*-expressing fibers might preferentially target specific tissue types. Indeed, a survey of recombination across different nerves and tissues suggested that the innervation of some tissues by *KOR-cre* afferents might be greater than others (Figure S6). To assess this possibility, we back-labeled primary afferents that innervated the bladder, the colon, or skeletal muscle (Figures 4K and 4L) and performed single cell RT-PCR. *Oprk1* was detected in ~60% of colon afferents and ~50% of bladder afferents, but only 7% muscle afferents. Despite having distinct peripheral targets, *Oprk1*-positive afferents from all three of these tissues appeared rather uniform: 97% expressed *Calca*; 92% expressed *Tac1*; 95% expressed *Trpv1*; and 94% expressed *Trka*. These findings suggest that KOR defines a subtype of peptidergic afferent that is highly represented in visceral organs, such as colon and bladder.

KOR is functionally expressed in sensory neurons and mediates inhibition of voltage-gated Ca^{2+} currents

Previous studies have suggested that KOR agonists inhibit voltage-gated Ca^{2+} currents (VGCC) in a subpopulation of primary afferents (Bean, 1989; Macdonald and Werz, 1986; Su et al., 1998; Wiley et al., 1997). To confirm these observations, we measured the effects of the endogenous ligand dynorphin on VGCC through whole-cell patch clamp recordings on freshly dissociated DRG neurons. When recording from tdTomato-positive cells that were genetically labeled by the *KOR-cre* allele, we observed that dynorphin (0.1 and 1 μM) caused a significant decrease in VGCC, which returned to baseline upon washout (Figures 5A, 5B, S7A and S7B). Dynorphin treatment was also associated with a significant increase in current rise time (Figure S7C), consistent with the possibility that the inhibition of peak inward current reflects a KOR-induced rightward shift in the voltage-dependence of channel activation (Bean, 1989). Moreover, the effects were specific to KOR since the decrease in current caused by dynorphin was blocked by the KOR antagonist nor-BNI (Figures 5A, 5B and S7D). In contrast, primary afferents that were not genetically labeled by the *KOR-cre* allele showed neither a decrease in the magnitude of VGCC nor an increase in rise time upon application of dynorphin (Figures 5B, S7B and S7C).

Human DRG neurons that express KOR are also peptidergic and KOR agonists decrease Ca^{2+} influx in these neurons

For translational relevance, we next performed single-cell RT-PCR on freshly dissociated DRG neurons obtained from human organ donors. *Oprk1* mRNA was detected in ~1/4 of the human afferents (5 of 20 cells/two donors), and all the *Oprk1*-positive cells expressed the classical peptidergic transcripts *CALCa*, *TRPV1*, and *GFRa3* (Figure 5C), similar to what we observed in the mouse. To determine whether human DRG neurons expressed functional KOR, we used Ca^{2+} imaging to test the effects of dynorphin on the high K^+-evoked increase in intracellular Ca^{2+}. In 12 of 26 neurons tested, dynorphin caused a decrease in the evoked Ca^{2+} transient that was greater than 2 SD from the mean baseline response (Figures 5D and 5E). Together, these findings suggest that KOR is anatomically and functionally expressed in a subset of human peptidergic afferents.

Author Manuscript Author Manuscript Author Manuscript Author Manuscript

KOR decreases excitatory neurotransmission from primary afferents in the superficial and deep dorsal horn

To address the role of KOR on the central terminals of sensory neurons, we tested the effects of the dynorphin on the amplitude of light-evoked excitatory post-synaptic potentials (eEPSCs) that were observed upon optogenetic activation of *KOR-cre* afferents. To record from lamina I neurons, we used the *ex vivo* spinal cord preparation, (Figure 6A) (Hachisuka et al., 2016). First, we identified neurons that likely received monosynaptic input from *KOR-cre* afferents based on eEPSC latency and the absence of eEPSC failure following optogenetic stimulation of *KOR-cre* afferent input. Next, we analyzed the effect of dynorphin in paired-pulse recordings. These experiments revealed that dynorphin significantly and reversibly decreased eEPSC amplitude and increased the paired-pulse ratio, evoked by optogenetic stimulation of *KOR-cre* afferents (Figures 6B, 6C and 6D). Similar results were observed when the experiments were repeated in the presence of naltrexone (1 μm), indicating that they were not due to a dynorphin-induced activation of MOR (Figures S8A, S8B, S8C and S8D). These findings suggest that KOR reduces excitatory neurotransmission from the central terminals of *KOR-cre* primary afferents in the superficial dorsal horn, consistent with previous findings (Ikoma et al., 2007; Kohno et al., 1999; Randic et al., 1995).

To investigate whether the *KOR-cre* afferents that target the deep dorsal horn were similarly modulated by KOR signaling, we developed a modified spinal cord preparation in which a single parasagittal cut in one hemisphere of the spinal cord was performed in order to target neurons in lamina III for patch-clamp recordings (Figure 6E). For these experiments, we applied blue light to the dorsal root to stimulate *KOR-cre* positive afferents expressing ChR2. We identified neurons in the dorsal horn that likely received monosynaptic input from these fibers by the absence of eEPSC failure following optogenetic stimulation of *KOR-cre* afferents. Just as observed in lamina I neurons, treatment with dynorphin caused a significant and reversible decrease in the first peak amplitude of eEPSCs in lamina III neurons that corresponded to a significant increase in the paired-pulse ratio (Figures 6F, 6G and 6H). Similar results were also obtained in the presence of naltrexone (1 μm) to block MOR (Figures S8E, S8F, S8G and S8H). Taken together, these findings suggest that KOR expressed at the central terminals of both nociceptors and LTMRs is functional and likely mediates presynaptic inhibition of both types of afferent input to the spinal cord dorsal horn.

KOR signaling inhibits neurogenic inflammation

Based on the finding that KOR is expressed in mouse and human peptidergic afferents, we sought to address whether KOR activation could inhibit neurogenic inflammation. To address this question, we measured plasma extravasation in mice that had received an intraplantar injection of capsaicin in the presence or absence of a KOR agonist (Figure 7A). For these experiments, we compared the effects of nalfurafine, a centrally-penetrating KOR agonist (Endoh et al., 1999; Nagase et al., 1998), to those of either ICI204,488 or FE200665 (Vanderah et al., 2008), two peripherally restricted KOR agonists that have extremely limited ability to cross the blood brain barrier (Figure 7C) (Shaw et al., 1989; Vanderah et al., 2008). In control mice, injection with the TRPV1 agonist capsaicin resulted in a significant increase in Evans blue in the ipsilateral paw relative to the contralateral paw. In

Author Manuscript Author Manuscript Author Manuscript Author Manuscript

contrast, treatment with any of the three KOR agonists significantly reduced capsaicin-induced plasma extravasation (Figures 7B and 7C). These observations are consistent with previous data (Green and Levine, 1992). Similar results were observed when neurogenic inflammation was induced with an inflammatory mixture of bradykinin and prostaglandin E2 (Figure S9). Importantly, we found that nalfurafine failed to attenuate Evans blue extravasation in *KOR−/−* mice, confirming that this inhibition is specific to KOR (Figure 7D). Finally, as an independent measure of neurogenic inflammation, we also assessed the effects of KOR agonists on the increase in paw temperature observed following capsaicin-injection into the hindpaw. Intraplantar injection of capsaicin in vehicle-treated mice resulted in an increase in paw temperature that was significantly attenuated in mice treated with either nalfurafine or ICI204,488 (Figures 7E and 7F). Together, these results suggest that activation of KOR in the periphery is sufficient to inhibit neurogenic inflammation.

KOR signaling in the periphery inhibits inflammatory mediator-induced sensitization of nociceptive afferents

To further assess the functional effects of peripheral KOR agonists, we performed single unit electrophysiological recordings of colonic nociceptive afferents (Figure 8A). Under baseline conditions, application of the KOR agonist nalfurafine to the receptive field of colonic afferents had no effect on the number of action potentials evoked by stretch of the colon (data not shown). However, KOR agonists reversed the sensitization of colonic afferents induced by inflammatory mediators (histamine, bradykinin, prostaglandin E2, and serotonin) (Figure 8B). To quantify this effect, we recorded the response to stretch in the presence of bath solution alone (baseline) on the receptive field, following application of inflammatory mediators (IM), and after application of inflammatory mediators together with nalfurafine (IM + Nalf). Inflammatory mediators increased the number of action potentials in response to stretch, whereas nalfurafine significantly reduced this sensitization (Figure 8C). In contrast, nalfurafine failed to reverse inflammatory mediator-induced sensitization in mice lacking *KOR* (Figure S10). In particular, a nalfurafine-mediated decrease in sensitization, as defined as a change in spikes greater than two SDs from the sensitized response, was common when recording from nociceptors from wild type mice (5 of 8 neurons) but absent in nociceptors from *KOR−/−* mice (0 of 6 neurons; $p < 0.05$, Fisher Exact test). Intriguingly, while nalfurafine reduced the number of action potentials (Figure 8C), it had no significant effect on the action potential threshold ($p > 0.05$; data analyzed with a one-way RM ANOVA on Ranks, Tukey post-hoc). These findings suggest that KOR signaling in the periphery reduces the gain of sensitized nociceptors, likely via second messenger pathways, rather than via direct inhibition of action potential generation.

Optogenetic activation of KOR-expressing primary afferents elicits withdrawal

Given the highly peptidergic nature of many KOR-expressing afferents, it seemed likely that selective activation of this population might elicit nociceptive withdrawal behaviors. To test this idea directly, we expressed ChR2 in *KOR-cre* mice using either a virus (FLEX.ChR2-tdt) or the Ai32 allele (Figure 9A). Blue light LED stimulation was applied to the glabrous hind paw skin. In control littermates (that had received the Cre-dependent virus but lacked *KOR-cre*), blue light stimulation did not elicit a withdrawal response at any intensity tested. In contrast, when ChR2 was expressed in *KOR-cre* afferents using either a virus or an allele,

Author Manuscript Author Manuscript Author Manuscript Author Manuscript

light stimulation of the hindpaw elicited a robust withdrawal response that was frequently accompanied by either jumping or licking/biting of the hindpaw, or both (Figure 9B). When blue light was applied to the shaved skin at the abdomen, thereby activating a mixed population of *KOR-cre* afferents (peptidergic and LTMRs), a startle response was observed most commonly, occasionally accompanied by licking, jumping or vocalization (Figure S11). These findings suggest that activation of KOR-expressing afferents results mainly in nocifensive responses.

Peripherally restricted KOR agonists inhibit chemical pain and itch behaviors, but not thermal thresholds.

Given that activation of KOR-expressing afferents appeared to be aversive, we next investigated whether inhibition of these cells with a KOR agonists would reduce responses to noxious stimuli. To do so, we compared the effects of nalfurafine to those of either ICI204,488 or FE200665 (Figure 9C). For these experiments, mice of both sexes were used and, since no difference between sexes was observed, data were pooled. Following an intraplantar injection of capsaicin, mice treated with any of the three KOR agonists showed a significant decrease in the time spent licking the injected hindpaw (Figure 7D) compared to mice treated with vehicle. Similarly, all three KOR agonists reduced the time that mice spent licking the injected hindpaw following an IPL injection of acetic acid (Figure 9E). Furthermore, both centrally active and peripherally restricted KOR agonists reduced scratching behavior in response to intradermal chloroquine (Figure 9F). Importantly, these effects were due to the action at KOR, rather than an off-target effect of the drugs, as nalfurafine, ICI204,448 or FE200665 at the doses used in this study had no effects in mice that lacked KOR (Figure S12). Taken together, these results suggest that peripherally restricted KOR agonists are sufficient to decrease acute responses to chemical irritants.

To determine the modality specificity of peripherally restricted KOR agonists, we next investigated their effects on mechanical and thermal sensitivity, both under naïve conditions and in a model of post-operative pain. In naïve mice, none of the KOR agonists had any effects on paw withdrawal threshold to the application of von Frey filaments (Figure 9G). Furthermore, nalfurafine, but not the peripherally restricted agonists ICI204,448 or FE200665, inhibited thermal responsivity in the Hargreaves' assay (Figure 9H).

Following injury, such as an incision during surgery, nociceptor activation and/or sensitization can drive ongoing pain and hypersensitivity to mechanical and thermal stimuli (Clark et al., 2006; Jang et al., 2011). To investigate whether KOR agonists might be useful for the management of post-operative pain, we used the Brennan incision model (Brennan et al., 1996) modified for use in mice (Pogatzki and Raja, 2003). With this model, we found that nalfurafine, ICI204,488, or FE200665 inhibited mechanical hypersensitivity following acute incision of the hindpaw (Figure 9I). In contrast, only nalfurafine, but not the peripherally restricted agonists, inhibited thermal hypersensitivity in the Brennan model (Figure 9J). Thus, whereas nalfurafine attenuated both thermal and mechanical hypersensitivity, peripherally restricted KOR agonists only inhibited mechanical sensitivity.

Author Manuscript Author Manuscript Author Manuscript Author Manuscript

DISCUSSION

Understanding which opioid receptors are expressed in different types of peripheral sensory neurons is important because this insight may inform the clinical use of peripherally restricted agonists. In the present study, we used the combination of a *KOR-cre* allele, viral tracing, single-cell RT-PCR, and electrophysiology to show that the KOR is expressed in, and attenuates signaling in, three main types of sensory neurons: a transcriptionally distinct subset of peptidergic afferents and two populations of low-threshold mechanoreceptors (LTMRs) whose peripheral terminals form either lanceolate or circumferential endings surrounding hair follicles. The peptidergic neurons are notable in that these afferents express particularly high levels of *Calca* and *Tac1* (the genes encoding CGRP and substance P, respectively), suggestive of a particularly important role in neurogenic inflammation. Consistent with this idea, we found that KOR agonists act in the periphery to attenuate afferent-evoked increases in plasma extravasation and blood flow and to reverse sensitization to inflammatory mediators.

An unexpected finding in our study is that the primary afferents that express KOR are not the ones that are currently thought to mediate itch (i.e., MrgprA3 or Nppb/SST populations) (Han et al., 2013; Mishra and Hoon, 2013). Yet, there is strong evidence that peripherally restricted KOR agonists inhibit itch as shown here and reported by others (Cowan et al., 2015; Inan and Cowan, 2004). Further work will be required to shed light on this apparent discrepancy. Nevertheless, it is noteworthy that many pruritogens (most famously histamine) induce wheal and flare that is thought to reflect the peripheral release of peptides (Groetzner and Weidner, 2010). Recently, substance P, which is released peripherally upon activation of peptidergic afferents, was shown to mediate itch via Mas-related G-protein coupled receptors on mast cells, resulting in their degranulation (Azimi et al., 2017). This finding raises the possibility that KOR agonists inhibit itch, at least in part, by reducing the peripheral release of substance P from KOR-expressing afferents, consistent with our plasma extravastion and thermography data. Alternatively, it is possible that KOR expression on immune cells is responsible for the anti-pruritic effects of peripherally selective KOR agonists. Although we did not detect *Oprk1* in dermal immune cells by RT-PCR or in situ hybridization, we acknowledge this message may be expressed at low levels that could be hard to detect.

One of the interesting findings in our study was that peripherally restricted and centrally penetrant KOR agonists had distinct effects: only nalfurafine reduced heat thresholds in the Hargreaves' test in either naïve mice or following incision, consistent with the idea that these effects of KOR are central rather than peripheral in origin. In contrast, both peripherally restricted and centrally penetrant KOR agonists reduced nocifensive behavior and neurogenic inflammation upon intraplantar injection of a TRPV1 agonist. The observation that peripherally restricted KOR agonists attenuated the response to capsaicin yet failed to influence the heat hyperalgesia following incision is noteworthy. We suggest that the distribution of KOR among peptidergic afferents may hold the explanation for these results: peptidergic afferents lacking KOR may be responsible for heat hyperalgesia, while peptidergic afferents expressing KOR may play a more dominant role in neurogenic

Author Manuscript Author Manuscript Author Manuscript Author Manuscript

inflammation, which indirectly contributes to the mechanical sensitivity observed in the incision model.

The results from the present study agree with and extend upon previous efforts aimed at testing whether activation of KOR in the periphery is an effective strategy for pain management. Previous studies have revealed that local application of KOR agonists (using doses that would not be effective systemically) reduces pain in response to formalin, Complete Freund's Adjuvant (CFA) and prostaglandin E2 (Antonijevic et al., 1995; Auh and Ro, 2012; Binder et al., 2001; Cunha et al., 2012; Keita et al., 1995; Obara et al., 2009; Stein et al., 1989). Furthermore, peripherally restricted KOR agonists have been found to reduce nociceptive behavior in response to formalin and CFA, as well as acetic acid-induced writhing, and chloroquine-induced itch (Barber et al., 1994; Binder and Walker, 1998; Caram-Salas et al., 2007; Inan and Cowan, 2004; Vanderah et al., 2008; Vanderah et al., 2004). Our work builds upon these studies with the incision model, which is likely to be relevant for the clinical application of these compounds, and by directly comparing the effects of a KOR agonist that penetrates centrally to that those that are peripherally restricted. Critically, we show that the KOR agonists tested here (nalfurafine, ICI204,488 and FE200665) are specific to KOR at the doses used, as they had no effect on pain and itch behaviors in *KOR*$^{-/-}$ mice. Moreover, we show for the first time that human primary afferents are inhibited by dynorphin, and that (just as we found in mouse) the subset that expresses KOR are peptidergic. These experiments are highly pertinent because there is currently great interest in the therapeutic potential of peripherally selective KOR agonists, with several groups performing clinical trials. Thus far, this approach appears promising, with significant analgesic or anti-pruritic effects observed in five different Phase 2 studies for post-operative pain, arthritic pain, and uremic pruritus using a tetrapeptide KOR agonist (CR845), which is very similar to the one used in our study (FE200665). Thus, peripherally selective KOR agonists may be a promising therapeutic approach to reduce pain, itch and neurogenic inflammation without central side-effects.

STAR METHODS

Contact for Reagent and Resource Sharing

Further information and requests for resources and reagents should be directed to and will be fulfilled by the corresponding authors and Lead Contacts, Dr. Sarah E. Ross (saross@pitt.edu), Dr. H Richard Koerber (rkoerber@pitt.edu) or Dr. Michael S. Gold (msg@pitt.edu)

Experimental Model and Subject Details

Animals—Mice were given free access to food and water and housed under standard laboratory conditions. The use of animals was approved by the Institutional Animal Care and Use Committee of the University of Pittsburgh.

Human Tissue—L4 and L5 DRG from four donors were collected with the consent of family members for the use of their loved one's tissue for research purposes. The protocol

Author Manuscript Author Manuscript Author Manuscript Author Manuscript

for the collection and study of tissue from organ donors was approved by the University of Pittsburgh Committee for Oversight of Research and Clinical Training Involving Decedents.

Method Details

Animal Husbandry—*KOR-cre* mice were generated as previously described and are maintained on a mixed C57bl/6.129J background (Cai et al., 2016). For some electrophysiological and anatomical experiments, *KOR-cre* mice were mated with Ai9 (Cre-responsive tdTomato reporter) mice or with Ai32 (Cre-responsive ChR2-eYFP) mice (The Jackson Laboratory). For most behavioral experiments 5 – 8-week-old male and female C57bl/6 mice were used. For some behavioral experiments, heterozygous *KOR-cre−/+* mice were harem mated and age-matched wild-type and *KOR-cre−/−* male and female offspring from the resulting litters were used. In all cases, no differences between male and female mice were observed and so the data were pooled.

Intrathecal injections—Intrathecal injections were performed as previously described (Kardon et al., 2014). Mice were anesthetized with isoflurane in a flow of O2 and the hair on their back was clipped. All intrathecal injections were delivered in a total volume of 5 μl using a 30-gauge needle attached to a luer-tip 25 μL Hamilton syringe. The needle was inserted into the tissue at a 45° angle and through the fifth intervertebral space (L5 – L6) causing a sudden lateral movement of the tail. Solution was injected at a rate of 1 μL/s. The needle was held in position for 10 s and removed slowly to avoid any outflow of the solution. Anesthesia was discontinued and the mice recovered from anesthesia within 5 min.

Histology

Immunofluorescence—Mice were deeply anaesthetized and fixed by perfusion with 4% paraformaldehyde. After tissue was collected, tissue was post-fixed in 4% PFA rinsed in 1X PBS, placed in 30% sucrose at 4 °C overnight. Then 20 μm thick sections were cut with a cryostat (Leica), mounted onto Superfrost Plus slides (Fisher Scientific) and stored at −20 °C until use. Tissue sections were blocked in 10% donkey serum and 0.25% Triton-X in PBS for 1 h at room temperature. Sections were incubated with primary antibodies in block overnight at 4 – 8 °C. Slides were washed 4 × 5 min in PBS containing 0.1% triton-X. Primary antibodies were revealed with species-specific secondary antibodies raised in donkey and conjugated to Pacific Blue, Alexa488, Alexa555, or Alexa647 (Life Technologies) diluted at 1:500 in block, washed as above, and coverslipped. The primary antibodies used were: sheep anti-CGRP (1:2000, Abcam), rabbit anti-NF200 (1:1000, Sigma Aldrich), mouse anti-NF200 (1:500, Sigma Aldrich), rabbit anti-TH (1:1000, Millipore), mouse anti-parvalbumin (1:1000, Millipore), rabbit anti-PGP9.5 (1:1000, UltraClone Limited), rabbit anti-substance P (1:10000, Immunostar), goat anti-TRPV1 (1:1000, Santa Cruz Biotechnologies), rabbit anti-RFP (1:1000, Rockland), and rabbit anti-TRPM8 (1:500, gift from M. Tominaga, Okazaki Institute for Integrative Bioscience). IB4 binding was visualized using biotinylated IB4 (Sigma, 1:500) and fluorophore-conjugated streptavidin (Life Technologies, 1:500) in place of primary and secondary antibodies. Slides were imaged using a Nikon A1R confocal microscope through either a 20x or 60x oil-immersion lens. Full-tissue thickness z-stacks (0.5–1 μm sections) were taken. All images are representative maximum intensity projections of 2 μm thickness (2 – 4 individual z-stacks).

Author Manuscript Author Manuscript Author Manuscript Author Manuscript

Quantification—For quantification of co-localization of *KOR-cre* positive neurons, full-tissue thickness z-stack images of lumbar (L1 - L6) DRGs were analyzed. At least seven individual sections DRG were analyzed per mouse for each marker analyzed, and at least 3 mice were analyzed per developmental time point. Sections of DRG analyzed were at least 100 μm apart in order to avoid counting a single neuron multiple times, and only neurons with visible nuclei were counted. Neurons were counted using Nikon Elements Advanced Research Software.

In Situ Hybridization—Mice were deeply anaesthetized, fixed by perfusion with 4% paraformaldehyde and lumbar DRG were collected and placed directly in 30% sucrose solution at 4 °C overnight. Tissues were embedded in OCT, sectioned at 12 μm, collected on Superfrost Plus slides (Fisher Scientific), and stored at −80 °C until use. RNAscope Multiplex Fluorescent Assay. Slides were washed in PBS for 5 min and pretreated per manufacturer's instructions. Protease treatment was applied for 15 min at 40 °C. Target probes for *Oprk1* and *tdTomato* were combined and hybridized for 2 h at 40 °C using the HybEZ Hybridization System. Following amplification and label application, slides were imaged with a Leica TCS SPE confocal microscope. 63x (no zoom) full-tissue thickness z-stacks (~2 μm sections) were taken. A threshold of 4 mRNA molecules was set for a positive count.

Isolation and plating of human sensory neurons

DRG were obtained from organ donors following collection of tissue needed for transplantation purposes as previously described (Zhang et al., 2015). Following surgical isolation of ganglia, they were placed in ice cold collection media composed of (in mM) 124.5 NaCl, 5 KCl, 1.2 $MgSO_4$, 1 $CaCl_2$, and 30 HEPES, and had been filter sterilized after the pH had been adjusted to 7.35 with NaOH. The time between cross-clamp and the harvest of ganglia was generally under 45 min, and the time between tissue collection and initiating the dissociation protocol was less than three hours. The protocol and combination of solutions employed were as previously (Zhang et al., 2015) except that the complete media used for plating the neurons consisted of basal media (500 ml bottle of L-15 media containing (in mg): 60 imidizole, 15 aspartic acid, 15 glutamic acid, 15 cystine, 5 β-alanine, 10 myo-inositol, 10 cholineCl, 5 p-aminobenzoic acid, 25 fumaric acid, 2 vitamin B12 and 5 of lipoic acid (which was first dissolved in methanol at a concentration of 1g/2.5 ml)) diluted with fetal bovine serum (1:10) and then supplemented to yield a final concentration of 50 ng/mL nerve growth factor (NGF 2.5S, Invitrogen), 0.3 mg/mL glutamine (Invitrogen), 4.5 mg/mL glucose (Sigma-Aldrich), 0.525 mg/mL ascorbic acid (Sigma-Aldrich), 2.4 mg/mL glutathione (Invitrogen), and 0.2% (w/v) $NaHCO_3$ (Sigma-Aldrich). Cells were plated onto poly-L-lysine coated glass coverslips (Invitrogen) placed in 35 mm culture dishes and stored in a CO_2 (5%) incubator at 37 ˚C for 2 – 4 h prior to flooding the culture dishes with Complete Media. Neurons were studied within 12 h (acute) of plating.

Ca^{2+} Imaging

Neurons were incubated with 2.5 μm Ca^{2+} indicator fura-2 AM ester with 0.025% Pluronic F-127 for 20 min at room temperature. They were then labeled with FITC-conjugated IB4 (10 μg/mL) for 10 min at room temperature. Labeled neurons were placed in a recording

Author Manuscript Author Manuscript Author Manuscript Author Manuscript

chamber and superfused continuously with normal bath solution in mM 130 NaCl, 3 KCl, 2.5 $CaCl_2$, 0.6 $MgCl_2$, 10 HEPES, and 10 glucose, pH 7.4 (osmolality 325 mOsm). Fluorescence data were acquired on a personal computer running Metafluor software (Molecular Devices) via a CCD camera (model RTE/CCD 1300; Roper Scientific). The ratio of fluorescence emission (510 nm) in response to 340/380 nm excitation (controlled by a lambda 10–2 filter changer; Sutter Instruments) was acquired at 1 Hz during drug application. All drugs were applied through a computer-controlled peizo-driven perfusion system (switching time, <20 ms; fast-step model SF-77B; Warner Instruments). $[Ca^{2+}]i$ was determined from the fura-2 ratio after the in situ calibration experiment as described in detail previously (Scheff et al., 2013).

Electrophysiology

Patch clamp recordings from dissociated DRG neurons—Mice (5 – 8 weeks old) were deeply anesthetized and transcardially perfused with ice-cold Ca^{2+}/Mg^{2+}-free HBSS (Invitrogen). Bilateral DRG (L2 – L5) were dissected into cold HBSS and dissociated as described previously (Malin et al., 2007). Cells were plated in DMEM F-12 (Invitrogen) containing 10% fetal bovine serum (FBS) and antibiotics (penicillin/streptomycin, 50 U/mL). Two hours later, coverslips were flooded with Ca^{2+}/Mg^{2+}-free HBSS (Invitrogen) containing 5 mM HEPES and stored at room temperature. Experiments were performed within 8 h of tissue harvest.

Borosilicate glass electrodes were filled with (in mM) 100 Cs-methanesulfonate, 5 Na-methanesulfonate, 40 TEA-Cl, 1 $CaCl_2$, 2 $MgCl_2$, 10 HEPES, 11 EGTA, 2 Mg-ATP, and 1 Li-GTP, pH 7.2 (adjusted with Tris-base), 310 mOsm (adjusted with sucrose). Neurons were continuously superfused with a bath solution that contained (in mM) 100 Choline-Cl, 30 TEA-Cl, 2.5 $CaCl_2$, 0.6 $MgCl_2$, 10 HEPES, and 10 glucose, pH 7.4 (adjusted with Tris-base), 320 mOsm (adjusted with sucrose). Currents were evoked up to three times from each neuron before, during, and after drug application with the following voltage-clamp protocol: 50 ms, 70 mV steps from a holding potential of −70 mV to 0 mV. Series resistance compensation (>70%) was used for all voltage-clamp recordings. To reduce the impact of leak currents, a p/4 leak subtraction protocol was used with a holding potential of −90 mV during the acquisition of the leak pulses.

Extracellular single-fiber recordings—Recordings were performed as previously described (McIlwrath et al., 2007). Briefly, Mice (4 – 6 weeks old) were deeply anesthetized, the hindlimb was shaved, and mice were perfused transcardially with oxygenated 6 °C sucrose-based artificial cerebral spinal fluid (ACSF) in mM: 39.0 sucrose, 0.9 KCl, 1.2 KH_2PO_4, 1.3 $MgSO_4$, 2.4 $CaCl_2$, 26.0 $NaHCO_3$, 10.0 D-glucose. The saphenous nerve and its innervation field were excised, transferred to a dual chamber recording dish, superfused with chilled oxygenated synthetic interstitial fluid (SIF) in mm: 123.0 NaCl, 3.5 KCl, 0.7 $MgSO_4$, 1.7 NaH_2PO_4, 2.0 $CaCl_2$, 9.5 sodium gluconate, 5.5 glucose, 7.5 sucrose, 10 HEPES, pH 7.4, and warmed slowly to 31 °C. The skin was pinned epidermal-side up on a rigid perforated metal platform, and the level of the circulating SIF was adjusted to bathe the corium side from underneath. This allowed for mechanical and optical stimulation of the dry skin (adapted from (Koerber and Woodbury, 2002)). The

Author Manuscript Author Manuscript Author Manuscript Author Manuscript

saphenous nerve was threaded into a mineral oil-filled recording chamber and placed on top of a small mirror for dissection. The nerve was de-sheathed and extracellular recordings were obtained from functionally identified single myelinated fibers in teased filaments draped over a silver hook electrode (Kress et al., 1992; Reeh, 1986). Signals were amplified, digitized, and recorded using Spike2 software for offline analysis.

Once an individual fiber was isolated, its receptive field (RF) was located using a small brush and tested for light responsiveness using a blue laser (473 nm). Conduction velocity was assessed using a concentric electrode in the RF (distance to electrode/stimulus-response delay). Myelinated fibers were defined as conducting faster than 1 m/s (Koltzenburg et al., 1997). A feedback-controlled constant force stimulator (Dual Mode Lever System, Aurora Scientific, Aurora) with a 1-mm diameter contact area was used to determine mechanical threshold of the cell and to characterize its response to suprathreshold stimuli. Constant force stimuli consisting of square waves of 5 sec duration were applied in an ascending series of 1, 5, 10, 25, 50, and 100 mN with 30-s interstimulus intervals.

Patch clamp recordings from dorsal horn neurons—Mice (4 – 7 weeks old) were deeply anesthetized and perfused transcardially with ice-cold oxygenated (95% O_2 and 5% CO_2) sucrose-based artificial cerebrospinal fluid (ACSF) (in mM; 234 sucrose, 2.5 KCl, 0.5 $CaCl_2$, 10 $MgSO_4$, 1.25 NaH_2PO4, 26 $NaHCO_3$, 11 Glucose). The thoracolumbar spinal cord was placed into a small chamber containing ice-cold oxygenated sucrose-based ACSF. For lamina I recordings, the dural and pial membranes were carefully removed and the spinal cord was pinned onto a Sylgard block with the right dorsal horn facing upward with the recording chamber and transferred to the rig. For lamina III recordings, the L3 and L4 dorsal roots were kept such that they were at least 8 mm in length. Then, a single parasaggital cut was made using a vibratome (Leica) to expose the gray matter, but not cut the dorsal root entry zone. The spinal cord was then pinned onto the Sylgard block with the sectioned surface facing upward in the recording chamber. For both recording types, the preparation was perfused with normal ACSF solution (in mM; 117 NaCl, 3.6 KCl, 2.5 $CaCl_2$, 1.2 $MgCl_2$, 1.2 NaH_2PO4, 25 NaHCO3, 11 glucose) saturated with 95% O_2 and 5% CO_2 at 32 ˚C. Tissue was rinsed with ACSF for at least 30 min prior to recordings to wash out sucrose.

Neurons were visualized using a fixed stage upright microscope (BX51WI Olympus microscope) equipped with a 40x water immersion objective lens, a CCD camera (ORCA-ER Hamamatsu Photonics; XM10-IR, Olympus) and monitor screen. A narrow beam infrared LED (L850D-06 Marubeni, emission peak, 850 nm) was positioned outside the solution meniscus, as previously described (Safronov et al., 2007); Szucs, 2009 #55; Hachisuka, 2016 #50}. Whole-cell patch-clamp recordings were made with a pipette constructed from thin-walled single-filamented borosilicate glass that was filled with an intracellular solution containing the following (in mM): 135 K-gluconate, 5 KCl, 0.5 $CaCl_2$, 5 EGTA, 5 HEPES, 5 MgATP, pH 7.2. Signals were acquired with an amplifier (Axopatch 200B, Molecular Devices). The data were low-pass filtered at 2 kHz and digitized at 10 kHz with an A/D converter (Digidata 1322A, Molecular Devices; Power1401–3, CED) and stored using a data acquisition program (Clampex version 10, Molecular Devices or Signal 6, CED). The liquid junction potential was not corrected. Cell recordings were made in

Author Manuscript Author Manuscript Author Manuscript Author Manuscript

voltage-clamp mode at holding potentials of −70 mV to record excitatory postsynaptic currents (EPSCs). Blue light (GFP filter, centered around 485 nm, Lambda DG-4, Sutter instruments) was applied through the objective lens (x40) of the microscope. Light power on the sample was 1.3 mW/mm-2. The shutter was controlled by Clampex or Signal 6 software. Drugs were dissolved in ACSF and applied by exchanging solutions via a three-way stopcock.

Ex vivo colon-pelvic nerve single fiber recording—The colon-nerve recordings were performed as described previously (Feng et al., 2015). In brief, adult mice were euthanized via isoflurane overdose. Next, 4–5 cm of colon-rectum attached to pelvic nerve was removed intact and opened along the antimesenteric border and held muscosal side up in a chamber coated with Sylgard (Down Corning Corp., Midland, MI). The pelvic nerve was placed in a separate compartment, isolated via a grease gap filled with paraffin oil. The colon-rectum was superfused with a modified Krebs solution (in mM): 117.9 NaCl, 4.7 KCl, 25 $NaHCO_3$, 1.3 NaH_2PO_4, 1.2 $MgSO_4$ $(H_2O)_7$, 2.5 $CaCl_2$, 11.1 D-Glucose, 2 sodium butyrate and 20 sodium acetate, with added nifedipine (1 mM) and indomethacin (3 mM). This solution was bubbled with carbogen (O_2 95% and CO_2 5%) to reach a pH of 7.2–7.4 at 31–33 °C.

The pelvic nerve was teased into 6–10 bundles placed individually on a platinum recording electrode. The colonic afferent activity was amplified (x 10,000 times), filtered (0.3 kHz-10 kHz), sampled at 20 kHz using a 1401 interface (CED) and stored on a PC for further analysis.

The receptive field of muscular colonic afferent fibers were identified with an electrical stimulus (0.5-ms duration, 0.3 Hz) using a round-tipped concentric electrode (external diameter: 0.55 mm and internal diameter: 0.125 mm, FHC, Bowdoin, ME) where the receptive endings were localized as the site requiring minimum stimulus intensity to evoke an action potential. Mechanical sensitivity was then assessed by stroking the mucosal surface with a fine brush. All the afferents responded to von Frey hairs of 1 g and 0.4 g of force and 170 mN of circumferential stretch. Circumferential stretch was applied with a custom-built claw enabling uniform and highly reproducible stretch of the entire piece of colon via a servo-controlled force actuator (series 300B dual mode servo system, Aurora Scientific, Toronto, Canada). For the focal test solutions, a stainless-steel square (4 × 4 mm; height, 1 cm) chamber was placed over the receptive field and the Krebs solution was replaced with test solutions. Stretch stimuli were applied every three minutes. Solutions were exchanged between stimuli.

Back-labeling and single-cell RT-PCR

Back-labeling—Mice were anesthetized with isoflurane (2%) and fluorescent retrograde dyes (5 – 10 μL of Alexa Fluor-conjugated cholera toxin subunit beta (CTB) or wheat germ agglutinin (WGA)) were injected using a 31-gauge needle. For colon afferents, several small 2 μl injections were made beneath the serosal layer in the distal region of the colon, at the level of the base of the bladder. For bladder afferents, several 2 μl injections were made beneath the serosal layer in the urinary bladder body. To label muscle, injections were made

Author Manuscript Author Manuscript Author Manuscript Author Manuscript

into the femoral nerve. The incision was then sutured, and animals were allowed to recover before returning to their home cage.

Cell dissociation and pickup—Mice (5–8 weeks old) were deeply anesthetized and transcardially perfused with ice-cold Ca^{2+}/Mg^{2+}-free HBSS (Invitrogen). Bilateral DRG were dissected into cold HBSS and dissociated as previously described (Malin et al., 2007). Cells were plated onto laminin coated coverslips and then placed in culture conditions for 45 minutes to promote adhesion. Before pickup, cultures were flooded with cell collection buffer (in mM) 140 NaCl, 10 glucose, 10 HEPES, 5 KCl, 2 $CaCl_2$, 1 $MgCl_2$). Cells were picked up with borosilicate glass pipettes (World Precision Instruments) held by a 3-axis micromanipulator. Pipette tips were broken off into tubes containing 3 μL of lysis buffer (Epicentre, MessageBOOSTER kit), and stored at −80 °C until use.

Single cell amplification and qPCR—Transcripts from single cells were reverse transcribed and linearly preamplified using the MessageBOOSTER kit for cell lysate (Epicentre). After preamplification, the products were cleaned with RNA Cleaner & Concentrator-5 columns (Zymo Research) and transcript levels were quantified using qPCR with optimized primers and SsoAdvanced SYBR Green Master Mix (BioRad). Cycle-time (Ct) values were determined using regression. Quantification threshold was determined to be inter-replicate average of 35 Ct, the point where replicates have a 95% chance of reoccurring, and the GAPDH threshold for cell inclusion was set to 25 Ct to ensure we could detect transcripts a thousand-times less prevalent than *GAPDH*. If a cell met the criteria for inclusion, it would be corrected for primer efficiencies using the Pfaffl method (Pfaffl, 2001).

Evans blue extravasation—Male and female mice (8–12 weeks of age) were anesthetized with ketamine:xylazine (100:20 mg/kg). Mice were pretreated with a KOR agonist or vehicle delivered intraperitoneal. Five minutes later, Evans blue solution (50 mg/kg, 0.5%) was delivered via tail vein injection. Ten minutes later, capsaicin (10 μl of a 0.1% in a vehicle consisting of 5% Tween 80: 5% ethanol in PBS) was injected intraplantar into the mouse hindpaw. KOR agonists were delivered in the following concentrations: vehicle (PBS, 100 μL), nalfurafine 20 μg/kg, FE200665 (12 mg/kg), or ICI 204,488 (10 mg/kg). Mice were perfused with saline 5 minutes after intraplantar injection of the hindpaw, and the intraplantar tissue was harvested from hindpaws and incubated for 3 – 4 days in 500 μL DMSO at 50 ˚C. The solution was subsequently concentrated to 5 μL in DMSO. Hindpaw tissue was then desiccated at 67C. Solution was spun at 10,000 RPM for 20 min, and the concentration of Evans blue was measured using a spectrophotometer at 620 nm and fitted to a standard curve. Experiments were performed blinded to drug treatment.

Vasodilation during inflammation—Male and female mice (8–12 weeks of age) were anesthetized with urethane (1.5 – 2 g/kg). Drug or vehicle was delivered intraperitoneal fifteen minutes before injection of intraplantar injection of capsaicin (10 μl of a 0.1% solution in a vehicle consisting of 5% Tween 80: 5% ethanol in PBS) into the mouse hindpaw. Drugs were delivered in the following concentrations: vehicle (PBS, 100 μL), nalfurafine (20 μg/kg), or ICI 204,488 (10 mg/kg). The temperature of mice hindpaws was

Author Manuscript Author Manuscript Author Manuscript Author Manuscript

captured at a frequency of 1 Hz using a thermal imaging camera (A40 FLIR Systems) and temperatures recorded with ThermaCAM Researcher Pro 2.7 SR-1 software.

Behavior

All assays were performed and scored by an experimenter blind to treatment and/or genotype. Mice were pretreated with vehicle (sterile saline; 100 μL IP), nalfurafine (20 μg/kg; 100 μL IP), ICI 204,488 (10 mg/kg; 100 μL IP), FE200665 (12 mg/kg; 100 μL IP) fifteen minutes prior to testing. All testing was performed in the University of Pittsburgh Rodent Behavior Analysis Core.

Optogenetic withdrawal assay—Mice were placed in a clear plastic container on an elevated wire grid and allowed to acclimate for 60 min. The plantar surface of the hindpaw was stimulated with a targeted blue light LED beam (coolLED pE-100) for 1 s at either 1 mW, 3 mW, or 10 mW intensity. The number of responses out of ten applications per intensity was recorded. Both *KOR-cre−/−* mice and their wild-type littermates received an IP injection of AAV9.FLEX.ChR2-tdTomato.SVRE.WP40 at P1.

Acute itch behavior—The nape of the neck area was shaved at least twenty-four hours prior to the start of the experiment. Mice were placed in a clear plastic container (3.5” x 3.5” x 5”) for observation and allowed to acclimate for 30 min. An intradermal injection of chloroquine (200 μg/20 μL) was made into the nape of the neck. Mice were videotaped and the number of scratch bouts was counted during a thirty-minute observation period.

Acute chemical pain behavior—Mice were placed in a clear plastic container for observation and allowed to acclimate for 30 min. An intraplantar (IPL) injection of capsaicin (1.5%, 20 μL) or acetic acid (0.6%, 20 μL). Mice were videotaped and the amount of time spent licking the injected paw was quantified during a ten- or thirty-minute period, respectively.

Hargreaves’ test—Mice were placed in a clear plastic container on a glass floor maintained at 30 °C and allowed to acclimate for 60 min. A radiant heat beam was focused onto the hindpaw. The latency to hindpaw withdrawal was recorded with 3 trials per animal. Beam intensity was adjusted so that at baseline mice displayed a latency of 8 – 12 s. A cut-off latency of 30 s was set to avoid tissue damage.

von Frey test—Mice were placed in a clear plastic container on an elevated wire grid and allowed to acclimate for 60 min. The plantar surface of the hindpaw was stimulated with a set of calibrated von Frey filaments (0.008 – 6 g). The 50% paw withdrawal threshold was determined using the SUDO method (Bonin et al., 2014).

Post-operative pain assay—This assay was performed based on the original description in (Brennan et al., 1996) but adapted for use in mice as described in (Pogatzki and Raja, 2003). Mice were anesthetized (2.0% for induction and 1.5% for maintenance) with isoflurane in a flow of O_2, placed in a prone position. The left hindpaw was sterilized with betadine solution and wiped clean with sterile gauze. A 5-mm incision extending from the proximal edge of the heel towards the toes was made with a No. 11 scalpel. The incision was

Author Manuscript Author Manuscript Author Manuscript Author Manuscript

made through the glabrous skin, fascia and underlying plantaris muscle (leaving muscle origin intact). A single nylon mattress suture was used to close the wound and antibiotic ointment was applied to the area of the incision. Mice recovered from anesthesia within 5 min and were returned to their home cage. Two hours after the incision, mice were placed in clear plastic containers either on an elevated wire grid for von Frey testing or on a glass floor for Hargreaves' testing. Mechanical sensitivity was recorded as the number of withdrawal responses (out of 10) to a single von Frey fiber (vF # 3.61, 0.4 g) applied to the plantar surface of the paw adjacent to the incision. Thermal sensitivity was measured using the Hargreaves' test as described above, but the radiant heat beam was focused on the hindpaw near the area of the incision. Baseline measurements were made for both the von Frey and Hargreaves' tests twenty-four hours prior to the incision. Mice with wound dehiscence or puss around the incision at the time of behavioral testing were removed from the experiment.

Synthesis of FE200665—N^{α}- *tert*-butoxycarbonyl (Boc) and 2,2,4,6,7-pentamethyldihydro-benzofuran-5-sulfonyl (Pbf)-protected tetrapeptide (Boc-DPhe-DPhe-DNle-DArg(Pbf)-OH) was synthesized by standard solid phase synthesis using 9-fluorenylmethoxycarbonyl (Fmoc)-chemistry on chlorotrityl chloride resin. After completion of chain elongation, peptide was released by 1% trifluoroacetic acid (TFA) in dichloromethane and further coupled with 4-(aminomethyl)pyridine using Benzotriazol-1-yloxy tris (dimethylamino) phosphonium hexafluorophosphate (Bop) / N-Hydroxybenzotriazole (HOBt) / *N*-methyl morpholine in dimethylformamide for 2 h at room temperature. The protecting groups Boc and Pbf were simultaneously deblocked by 100% TFA for 3 h at room temperature, and the resulting peptide was purified by reverse phased-high performance liquid chromatography (RP-HPLC) to afford pure FE200665 in overall 62% yield.

Quantification and Statistical Analysis

Statistical analyses were performed using R or Prism7 software. Values are presented as mean ± SEM. Statistical significance was assessed using either students t-tests, a one-way ANOVA with Dunnett's post-hoc test, or a two-way ANOVA with General Linear Hypothesis test for repeated-measures with a significance level of 0.05. No statistical methods were used to determine sample sizes prior to experiments, but the sample sizes are similar to those typically used in the field.

Supplementary Material

Refer to Web version on PubMed Central for supplementary material.

ACKNOWLEDGEMENTS

We thank Dr. Makoto Tominga for the TRPM8 antibody, and the Penn Vector Core in the Gene Therapy Program of the University of Pennsylvania and the Sternson lab for provision of the original source material used to produce AAV9.CAGGS.Flex.ChR2-tdTomato.WPRE.SV40. Research reported in this publication was supported by NIH/NIAMSD grants AR063772 (S.E.R.), AR064445 (S.E.R), AR071720 (D.H.K.) and AR060744 (D.H.K.), NIH/NINDS grants NS023725 (H.R.K), NS096705 (H.R.K), NS092146 (L.M.S.) and NS735483 (L.M.S.), NS083347 (M.S.G.), and NS07433 (K.A.M), NIH/NIDA grants DA034975 (F.P.), DA041809 (F.P.), and DA031777 (G.S.), NIH/NIDDK grant DK107966 (M.S.G.), NIH/NIBIB grant EBO21877 (B.M.D.), NIH/OD grant OD023859 (B.M.D.; M. Howard, PD), DoD Neurosensory Research Award MR130053 (G.S.), DoD National Defense Science and Engineering Graduate (NDSEG) Fellowship (E.I.S.), and Rita Allen Foundation/American Pain Society Awards

Author Manuscript Author Manuscript Author Manuscript Author Manuscript

(S.E.R. and G.S.). T.H. was supported by JSPS Overseas Research Fellowships. G.S. is a New York Stem Cell Foundation—Robertson Investigator.

REFERENCES

Antonijevic I, Mousa SA, Schafer M, and Stein C (1995). Perineurial defect and peripheral opioid analgesia in inflammation. J Neurosci 15, 165–172. [PubMed: 7823127]

Auh QS, and Ro JY (2012). Effects of peripheral kappa opioid receptor activation on inflammatory mechanical hyperalgesia in male and female rats. Neurosci Lett 524, 111–115. [PubMed: 22819973]

Azimi E, Reddy VB, Pereira PJS, Talbot S, Woolf CJ, and Lerner EA (2017). Substance P activates Mas-related G protein-coupled receptors to induce itch. J Allergy Clin Immunol 140, 447–453.e443. [PubMed: 28219706]

Bai L, Lehnert BP, Liu J, Neubarth NL, Dickendesher TL, Nwe PH, Cassidy C, Woodbury CJ, and Ginty DD (2015). Genetic Identification of an Expansive Mechanoreceptor Sensitive to Skin Stroking. Cell 163, 1783–1795. [PubMed: 26687362]

Bailey CP, and Connor M (2005). Opioids: cellular mechanisms of tolerance and physical dependence. Curr Opin Pharmacol 5, 60–68. [PubMed: 15661627]

Barber A, Bartoszyk GD, Bender HM, Gottschlich R, Greiner HE, Harting J, Mauler F, Minck KO, Murray RD, Simon M, and et al. (1994). A pharmacological profile of the novel, peripherally-selective kappa-opioid receptor agonist, EMD 61753. Br J Pharmacol 113, 1317–1327. [PubMed: 7889287]

Basbaum AI (2008). The senses : a comprehensive reference (Amsterdam: Elsevier).

Bean BP (1989). Neurotransmitter inhibition of neuronal calcium currents by changes in channel voltage dependence. Nature 340, 153–156. [PubMed: 2567963]

Binder W, Machelska H, Mousa S, Schmitt T, Riviere PJ, Junien JL, Stein C, and Schafer M (2001). Analgesic and antiinflammatory effects of two novel kappa-opioid peptides. Anesthesiology 94, 1034–1044. [PubMed: 11465595]

Binder W, and Walker JS (1998). Effect of the peripherally selective kappa-opioid agonist, asimadoline, on adjuvant arthritis. Br J Pharmacol 124, 647–654. [PubMed: 9690855]

Bonin RP, Bories C, and De Koninck Y (2014). A simplified up-down method (SUDO) for measuring mechanical nociception in rodents using von Frey filaments. Mol Pain 10, 26. [PubMed: 24739328]

Boom M, Niesters M, Sarton E, Aarts L, Smith TW, and Dahan A (2012). Non-analgesic effects of opioids: opioid-induced respiratory depression. Curr Pharm Des 18, 5994–6004. [PubMed: 22747535]

Brennan TJ, Vandermeulen EP, and Gebhart GF (1996). Characterization of a rat model of incisional pain. Pain 64, 493–501. [PubMed: 8783314]

Cai X, Huang H, Kuzirian MS, Snyder LM, Matsushita M, Lee MC, Ferguson C, Homanics GE, Barth AL, and Ross SE (2016). Generation of a KOR-Cre knockin mouse strain to study cells involved in kappa opioid signaling. Genesis 54, 29–37. [PubMed: 26575788]

Caram-Salas NL, Reyes-Garcia G, Bartoszyk GD, Araiza-Saldana CI, Ambriz-Tututi M, Rocha-Gonzalez HI, Arreola-Espino R, Cruz SL, and Granados-Soto V (2007). Subcutaneous, intrathecal and periaqueductal grey administration of asimadoline and ICI-204448 reduces tactile allodynia in the rat. Eur J Pharmacol 573, 75–83. [PubMed: 17643411]

Chavkin C, James IF, and Goldstein A (1982). Dynorphin is a specific endogenous ligand of the kappa opioid receptor. Science 215, 413–415. [PubMed: 6120570]

Chavkin C, Sud S, Jin W, Stewart J, Zjawiony JK, Siebert DJ, Toth BA, Hufeisen SJ, and Roth BL (2004). Salvinorin A, an active component of the hallucinogenic sage salvia divinorum is a highly efficacious kappa-opioid receptor agonist: structural and functional considerations. J Pharmacol Exp Ther 308, 1197–1203. [PubMed: 14718611]

Clark JD, Qiao Y, Li X, Shi X, Angst MS, and Yeomans DC (2006). Blockade of the complement C5a receptor reduces incisional allodynia, edema, and cytokine expression. Anesthesiology 104, 1274–1282. [PubMed: 16732100]

Author Manuscript Author Manuscript Author Manuscript Author Manuscript

Cowan A, Kehner GB, and Inan S (2015). Targeting Itch with Ligands Selective for kappa Opioid Receptors. Handb Exp Pharmacol 226, 291–314. [PubMed: 25861786]

Cunha TM, Souza GR, Domingues AC, Carreira EU, Lotufo CM, Funez MI, Verri WA, Jr., Cunha FQ, and Ferreira SH (2012). Stimulation of peripheral kappa opioid receptors inhibits inflammatory hyperalgesia via activation of the PI3Kgamma/AKT/nNOS/NO signaling pathway. Mol Pain 8, 10. [PubMed: 22316281]

Dayton RD, Wang DB, and Klein RL (2012). The advent of AAV9 expands applications for brain and spinal cord gene delivery. Expert opinion on biological therapy 12, 757–766. [PubMed: 22519910]

de Nooij JC, Doobar S, and Jessell TM (2013). Etv1 inactivation reveals proprioceptor subclasses that reflect the level of NT3 expression in muscle targets. Neuron 77, 1055–1068. [PubMed: 23522042]

Endoh T, Matsuura H, Tajima A, Izumimoto N, Tajima C, Suzuki T, Saitoh A, Suzuki T, Narita M, Tseng L, and Nagase H (1999). Potent antinociceptive effects of TRK-820, a novel kappa-opioid receptor agonist. Life Sci 65, 1685–1694. [PubMed: 10573186]

Foust KD, Poirier A, Pacak CA, Mandel RJ, and Flotte TR (2008). Neonatal intraperitoneal or intravenous injections of recombinant adeno-associated virus type 8 transduce dorsal root ganglia and lower motor neurons. Hum Gene Ther 19, 61–70. [PubMed: 18052722]

Green PG, and Levine JD (1992). Delta- and kappa-opioid agonists inhibit plasma extravasation induced by bradykinin in the knee joint of the rat. Neuroscience 49, 129–133. [PubMed: 1328929]

Groetzner P, and Weidner C (2010). The human vasodilator axon reflex - an exclusively peripheral phenomenon? Pain 149, 71–75. [PubMed: 20138429]

Hachisuka J, Baumbauer KM, Omori Y, Snyder LM, Koerber HR, and Ross SE (2016). Semi-intact ex vivo approach to investigate spinal somatosensory circuits. eLife 5.

Han L, Ma C, Liu Q, Weng HJ, Cui Y, Tang Z, Kim Y, Nie H, Qu L, Patel KN, et al. (2013). A subpopulation of nociceptors specifically linked to itch. Nat Neurosci 16, 174–182. [PubMed: 23263443]

Horch KW, Burgess PR, and Whitehorn D (1976). Ascending collaterals of cutaneous neurons in the fasciculus gracilis of the cat. Brain Res 117, 1–17. [PubMed: 990925]

Ikoma M, Kohno T, and Baba H (2007). Differential presynaptic effects of opioid agonists on Adelta- and C-afferent glutamatergic transmission to the spinal dorsal horn. Anesthesiology 107, 807–812. [PubMed: 18073556]

Inan S, and Cowan A (2004). Kappa opioid agonists suppress chloroquine-induced scratching in mice. Eur J Pharmacol 502, 233–237. [PubMed: 15476749]

Jang JH, Liang D, Kido K, Sun Y, Clark DJ, and Brennan TJ (2011). Increased local concentration of complement C5a contributes to incisional pain in mice. J Neuroinflammation 8, 80. [PubMed: 21736743]

Ji RR, Zhang Q, Law PY, Low HH, Elde R, and Hokfelt T (1995). Expression of mu-, delta-, and kappa-opioid receptor-like immunoreactivities in rat dorsal root ganglia after carrageenan-induced inflammation. J Neurosci 15, 8156–8166. [PubMed: 8613750]

Kardon AP, Polgar E, Hachisuka J, Snyder LM, Cameron D, Savage S, Cai X, Karnup S, Fan CR, Hemenway GM, et al. (2014). Dynorphin acts as a neuromodulator to inhibit itch in the dorsal horn of the spinal cord. Neuron 82, 573–586. [PubMed: 24726382]

Keita H, Kayser V, and Guilbaud G (1995). Antinociceptive effect of a kappa-opioid receptor agonist that minimally crosses the blood-brain barrier (ICI 204448) in a rat model of mononeuropathy. Eur J Pharmacol 277, 275–280. [PubMed: 7493620]

Kieffer BL, and Gaveriaux-Ruff C (2002). Exploring the opioid system by gene knockout. Prog Neurobiol 66, 285–306. [PubMed: 12015197]

Koerber HR, and Woodbury CJ (2002). Comprehensive phenotyping of sensory neurons using an ex vivo somatosensory system. Physiol Behav 77, 589–594. [PubMed: 12527004]

Koltzenburg M, Stucky CL, and Lewin GR (1997). Receptive properties of mouse sensory neurons innervating hairy skin. J Neurophysiol 78, 1841–1850. [PubMed: 9325353]

Kress M, Koltzenburg M, Reeh PW, and Handwerker HO (1992). Responsiveness and functional attributes of electrically localized terminals of cutaneous C-fibers in vivo and in vitro. Journal of Neurophysiology 68, 581–595. [PubMed: 1527577]

Author Manuscript Author Manuscript Author Manuscript Author Manuscript

Lalanne L, Ayranci G, Kieffer BL, and Lutz PE (2014). The kappa opioid receptor: from addiction to depression, and back. Frontiers in psychiatry 5, 170. [PubMed: 25538632]

Le Pichon CE, and Chesler AT (2014). The functional and anatomical dissection of somatosensory subpopulations using mouse genetics. Frontiers in neuroanatomy 8, 21. [PubMed: 24795573]

Li L, Rutlin M, Abraira VE, Cassidy C, Kus L, Gong S, Jankowski MP, Luo W, Heintz N, Koerber HR, et al. (2011). The functional organization of cutaneous low-threshold mechanosensory neurons. Cell 147, 1615–1627. [PubMed: 22196735]

Macdonald RL, and Werz MA (1986). Dynorphin A decreases voltage-dependent calcium conductance of mouse dorsal root ganglion neurones. J Physiol 377, 237–249. [PubMed: 2432242]

Maekawa K, Minami M, Yabuuchi K, Toya T, Katao Y, Hosoi Y, Onogi T, and Satoh M (1994). In situ hybridization study of mu- and kappa-opioid receptor mRNAs in the rat spinal cord and dorsal root ganglia. Neurosci Lett 168, 97–100. [PubMed: 8028801]

Malin SA, Davis BM, and Molliver DC (2007). Production of dissociated sensory neuron cultures and considerations for their use in studying neuronal function and plasticity. Nature protocols 2, 152–160. [PubMed: 17401349]

McIlwrath SL, Lawson JJ, Anderson CE, Albers KM, and Koerber HR (2007). Overexpression of neurotrophin-3 enhances the mechanical response properties of slowly adapting type 1 afferents and myelinated nociceptors. Eur J Neurosci 26, 1801–1812. [PubMed: 17897394]

McKemy DD, Neuhausser WM, and Julius D (2002). Identification of a cold receptor reveals a general role for TRP channels in thermosensation. Nature 416, 52–58. [PubMed: 11882888]

Millan MJ (1990). Kappa-opioid receptors and analgesia. Trends Pharmacol Sci 11, 70–76. [PubMed: 2156363]

Mishra SK, and Hoon MA (2013). The cells and circuitry for itch responses in mice. Science 340, 968–971. [PubMed: 23704570]

Nagase H, Hayakawa J, Kawamura K, Kawai K, Takezawa Y, Matsuura H, Tajima C, and Endo T (1998). Discovery of a structurally novel opioid kappa-agonist derived from 4,5-epoxymorphinan. Chem Pharm Bull (Tokyo) 46, 366–369. [PubMed: 9501472]

Obara I, Parkitna JR, Korostynski M, Makuch W, Kaminska D, Przewlocka B, and Przewlocki R (2009). Local peripheral opioid effects and expression of opioid genes in the spinal cord and dorsal root ganglia in neuropathic and inflammatory pain. Pain 141, 283–291. [PubMed: 19147290]

Peier AM, Moqrich A, Hergarden AC, Reeve AJ, Andersson DA, Story GM, Earley TJ, Dragoni I, McIntyre P, Bevan S, and Patapoutian A (2002). A TRP channel that senses cold stimuli and menthol. Cell 108, 705–715. [PubMed: 11893340]

Pfaffl MW (2001). A new mathematical model for relative quantification in real-time RT-PCR. Nucleic Acids Res 29, e45. [PubMed: 11328886]

Pogatzki EM, and Raja SN (2003). A mouse model of incisional pain. Anesthesiology 99, 1023–1027. [PubMed: 14508341]

Porreca F, and Ossipov MH (2009). Nausea and vomiting side effects with opioid analgesics during treatment of chronic pain: mechanisms, implications, and management options. Pain Med 10, 654–662. [PubMed: 19302436]

Randic M, Cheng G, and Kojic L (1995). kappa-opioid receptor agonists modulate excitatory transmission in substantia gelatinosa neurons of the rat spinal cord. J Neurosci 15, 6809–6826. [PubMed: 7472439]

Reeh PW (1986). Sensory receptors in mammalian skin in an in vitro preparation. Neurosci Lett 66, 141–146. [PubMed: 3725179]

Safronov BV, Pinto V, and Derkach VA (2007). High-resolution single-cell imaging for functional studies in the whole brain and spinal cord and thick tissue blocks using light-emitting diode illumination. J Neurosci Methods 164, 292–298. [PubMed: 17586052]

Scheff NN, Lu SG, and Gold MS (2013). Contribution of endoplasmic reticulum Ca2+ regulatory mechanisms to the inflammation-induced increase in the evoked Ca2+ transient in rat cutaneous dorsal root ganglion neurons. Cell Calcium 54, 46–56. [PubMed: 23642703]

Seal RP, Wang X, Guan Y, Raja SN, Woodbury CJ, Basbaum AI, and Edwards RH (2009). Injury-induced mechanical hypersensitivity requires C-low threshold mechanoreceptors. Nature 462, 651–655. [PubMed: 19915548]

Author Manuscript Author Manuscript Author Manuscript Author Manuscript

Shaw JS, Carroll JA, Alcock P, and Main BG (1989). ICI 204448: a kappa-opioid agonist with limited access to the CNS. Br J Pharmacol 96, 986–992. [PubMed: 2568146]

Sheffler DJ, and Roth BL (2003). Salvinorin A: the “magic mint” hallucinogen finds a molecular target in the kappa opioid receptor. Trends Pharmacol Sci 24, 107–109. [PubMed: 12628350]

Shippenberg TS, Zapata A, and Chefer VI (2007). Dynorphin and the pathophysiology of drug addiction. Pharmacol Ther 116, 306–321. [PubMed: 17868902]

Smith DE (2017). Medicalizing the Opioid Epidemic in the U.S. in the Era of Health Care Reform. Journal of psychoactive drugs 49, 95–101. [PubMed: 28296623]

Smith HS, and Peppin JF (2014). Toward a systematic approach to opioid rotation. Journal of pain research 7, 589–608. [PubMed: 25378948]

Stein C, Millan MJ, Shippenberg TS, Peter K, and Herz A (1989). Peripheral opioid receptors mediating antinociception in inflammation. Evidence for involvement of mu, delta and kappa receptors. J Pharmacol Exp Ther 248, 1269–1275. [PubMed: 2539460]

Su X, Wachtel RE, and Gebhart GF (1998). Inhibition of calcium currents in rat colon sensory neurons by K- but not mu- or delta-opioids. J Neurophysiol 80, 3112–3119. [PubMed: 9862909]

Vanderah TW (2010). Delta and kappa opioid receptors as suitable drug targets for pain. Clin J Pain 26 Suppl 10, S10–15. [PubMed: 20026960]

Vanderah TW, Largent-Milnes T, Lai J, Porreca F, Houghten RA, Menzaghi F, Wisniewski K, Stalewski J, Sueiras-Diaz J, Galyean R, et al. (2008). Novel D-amino acid tetrapeptides produce potent antinociception by selectively acting at peripheral kappa-opioid receptors. Eur J Pharmacol 583, 62–72. [PubMed: 18282565]

Vanderah TW, Schteingart CD, Trojnar J, Junien JL, Lai J, and Riviere PJ (2004). FE200041 (D-Phe-D-Phe-D-Nle-D-Arg-NH2): A peripheral efficacious kappa opioid agonist with unprecedented selectivity. J Pharmacol Exp Ther 310, 326–333. [PubMed: 14993260]

Vulchanova L, Schuster DJ, Belur LR, Riedl MS, Podetz-Pedersen KM, Kitto KF, Wilcox GL, McIvor RS, and Fairbanks CA (2010). Differential adeno-associated virus mediated gene transfer to sensory neurons following intrathecal delivery by direct lumbar puncture. Mol Pain 6, 31. [PubMed: 20509925]

Werz MA, and Macdonald RL (1984). Dynorphin reduces voltage-dependent calcium conductance of mouse dorsal root ganglion neurons. Neuropeptides 5, 253–256. [PubMed: 6152324]

Wiley JW, Moises HC, Gross RA, and MacDonald RL (1997). Dynorphin A-mediated reduction in multiple calcium currents involves a G(o) alpha-subtype G protein in rat primary afferent neurons. J Neurophysiol 77, 1338–1348. [PubMed: 9084601]

Woodbury CJ, Ritter AM, and Koerber HR (2001). Central anatomy of individual rapidly adapting low-threshold mechanoreceptors innervating the “hairy” skin of newborn mice: early maturation of hair follicle afferents. J Comp Neurol 436, 304–323. [PubMed: 11438932]

Zhang XL, Lee KY, Priest BT, Belfer I, and Gold MS (2015). Inflammatory mediator-induced modulation of GABAA currents in human sensory neurons. Neuroscience 310, 401–409. [PubMed: 26415765]

Author Manuscript Author Manuscript Author Manuscript Author Manuscript

HIGHLIGHTS

- KOR is expressed in peptidergic primary afferents in mouse and human
- KOR is expressed in LTMRs that form circumferential and lanceolate endings
- KOR signaling inhibits nociceptor sensitization and neurogenic inflammation
- Peripherally selective KOR agonists inhibit nociception

Author Manuscript Author Manuscript Author Manuscript Author Manuscript

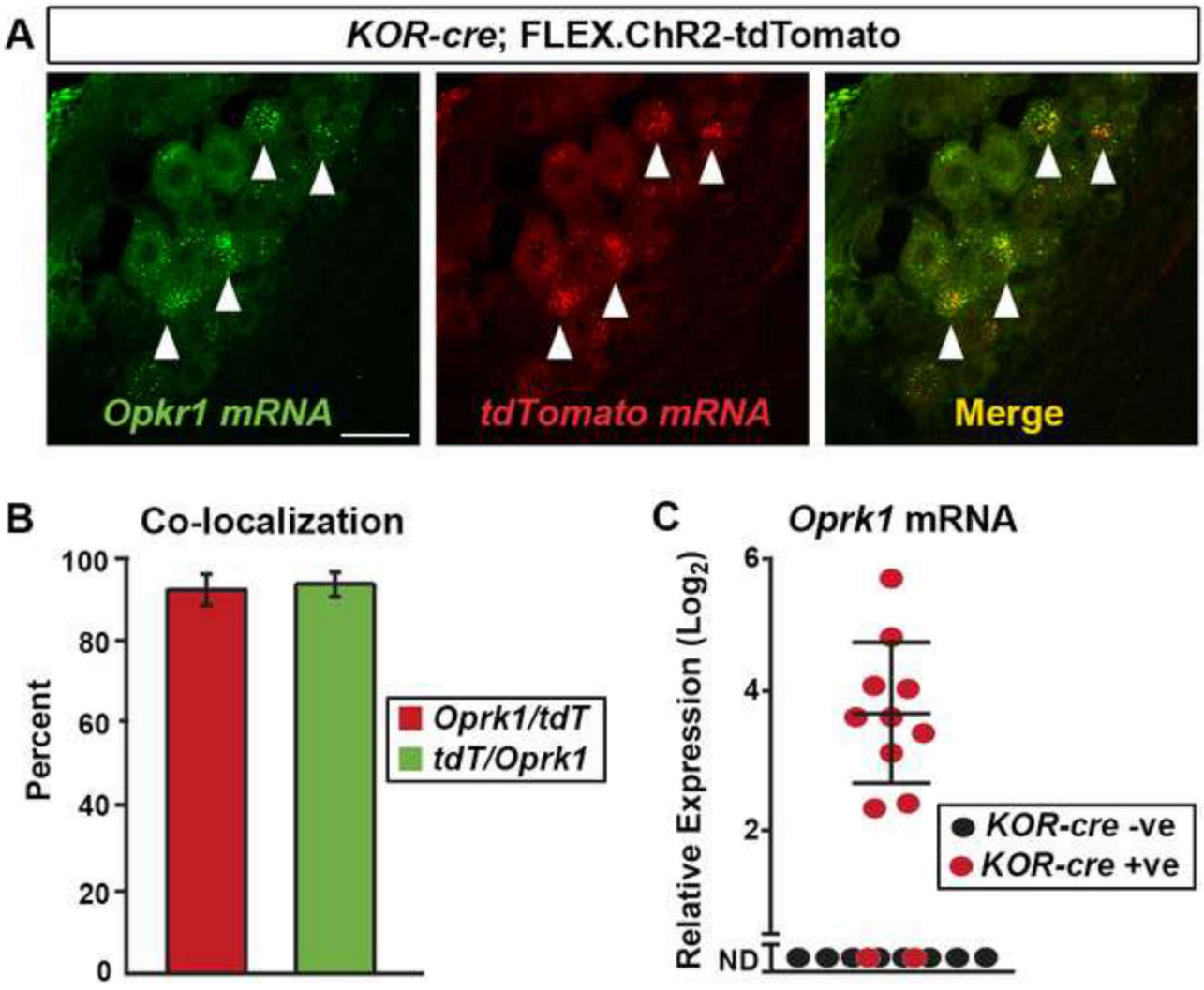

Figure 1. *KOR-cre* as a tool for targeting KOR-expressing dorsal root ganglia (DRG) neurons

A.Dual FISH of *Oprk1* (green) and *tdTomato* mRNA (red) shows high co-expression (merge) in DRG neurons. Lumbar DRG neurons were infected with the Cre-dependent virus (AAV.FLEX.ChR2-tdTomato) via IT injection at P40. Arrowheads indicate cells co-expressing *Oprk1* and *tdTomato* mRNA. Scale bar = 25 μm.

B. Quantification of (A). Most *tdTomato* positive neurons (red) co-expressed *Oprk1* mRNA, and most *Oprk1* postitive neurons (green) co-expressed *tdTomato.* n = 3 mice. Data are presented as mean ± SEM.

C. Single-cell RT-PCR of lumbar DRG neurons. *KOR-cre* mice were infected with an AAV.FLEX.ChR2-tdTomato virus via IT injection at P40. The majority of *KOR-cre;* AAV.FLEX.ChR2-tdtomato positive neurons (red dots) express detectable levels of *Oprk1* mRNA (10 of 12), while none (0 of 22) of the *KOR-cre* negative neurons (black dots) express detectable levels of *Oprk1* mRNA (only 8 cells are shown for clarity; ND, not detected). Data are presented as the $-\log_2 \Delta CT$ expression relative to *GAPDH* expression within the same cell such that larger numbers represent higher mRNA expression. Dots represent values from individual cells.

Author Manuscript Author Manuscript Author Manuscript Author Manuscript

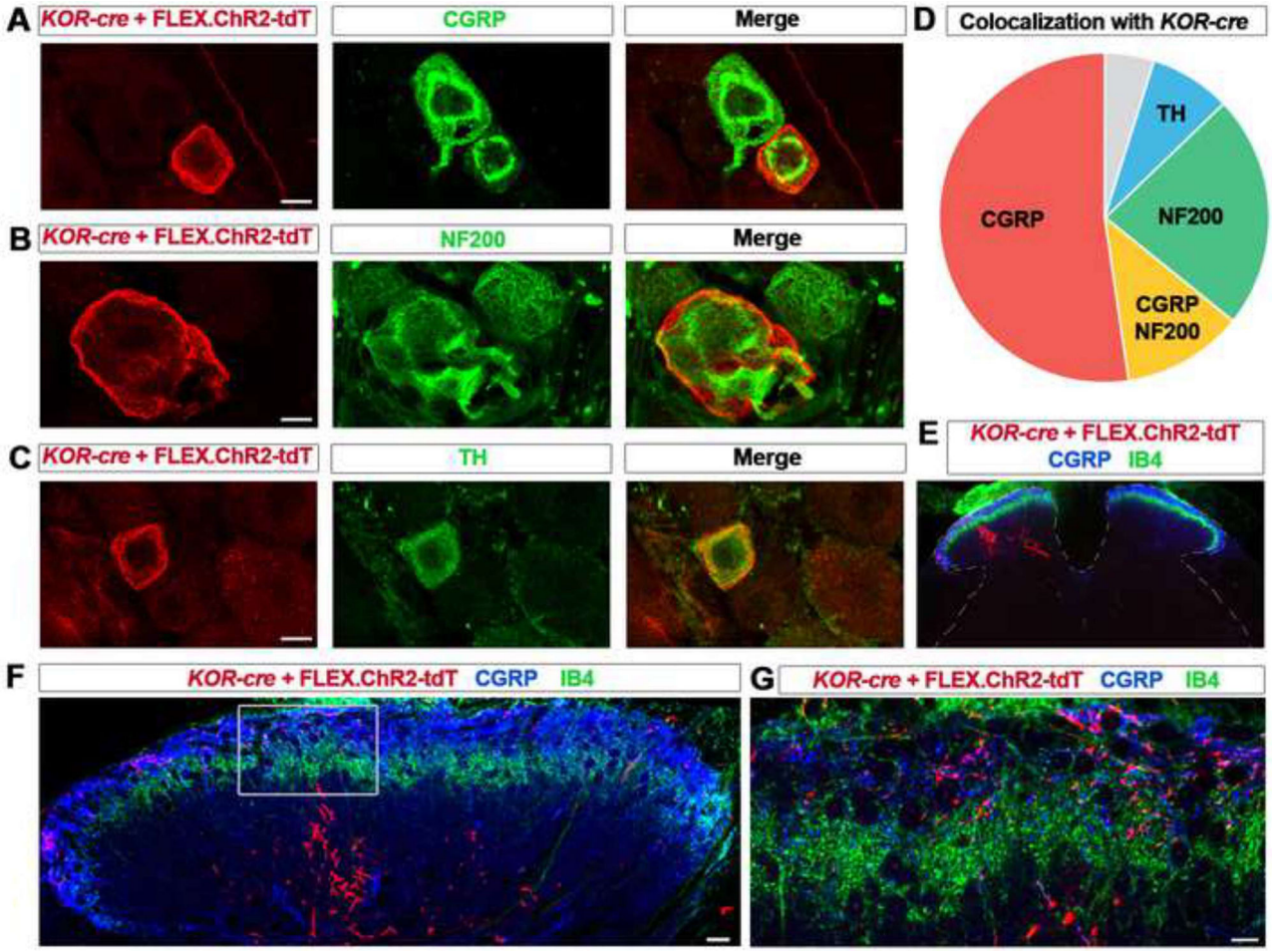

Figure 2. *KOR-cre* labels distinct neurochemical and anatomical subsets of primary afferents

A – C. IHC of lumbar DRG neurons from *KOR-cre* mice labeled using a Cre-dependent virus (AAV.FLEX.ChR2-tdTomato; IT in adult) and co-stained with antibodies to CGRP (A), NF200 (B), and TH (C). Scale bar = 10 μm.

D. Pie chart representing co-localization of immunohistochemical markers with virally-labeled (AAV.FLEX.ChR2-tdTomato, IT in adult) *KOR-cre* DRG neurons. 52% ± 5% of *KOR-cre* neurons co-localize with CGRP (red), 12% ± 6% co-localize with both CGRP and NF200 (yellow), 23 ± 6 % co-localize with NF200 (green), and 8% ± 2% co-localize with TH (blue). Only 5% ± 5% of *KOR-cre* neurons did not co-localize with any of these three markers (gray; n = 3 mice).

E – F. Representative images of lumbar spinal cord section of a *KOR-cre* mouse following an injection of AAV.FLEX.ChR2-tdTomato into the left sciatic nerve at P40. *KOR-cre* + FLEX.ChR2-tdt primary afferent terminals can be seen ipsilateral to the injection in the dorsal horn (E) in both the deeper dorsal horn below the IB4 band (F) and in the superficial dorsal horn where they co-localize with CGRP (G).

Author Manuscript Author Manuscript Author Manuscript Author Manuscript

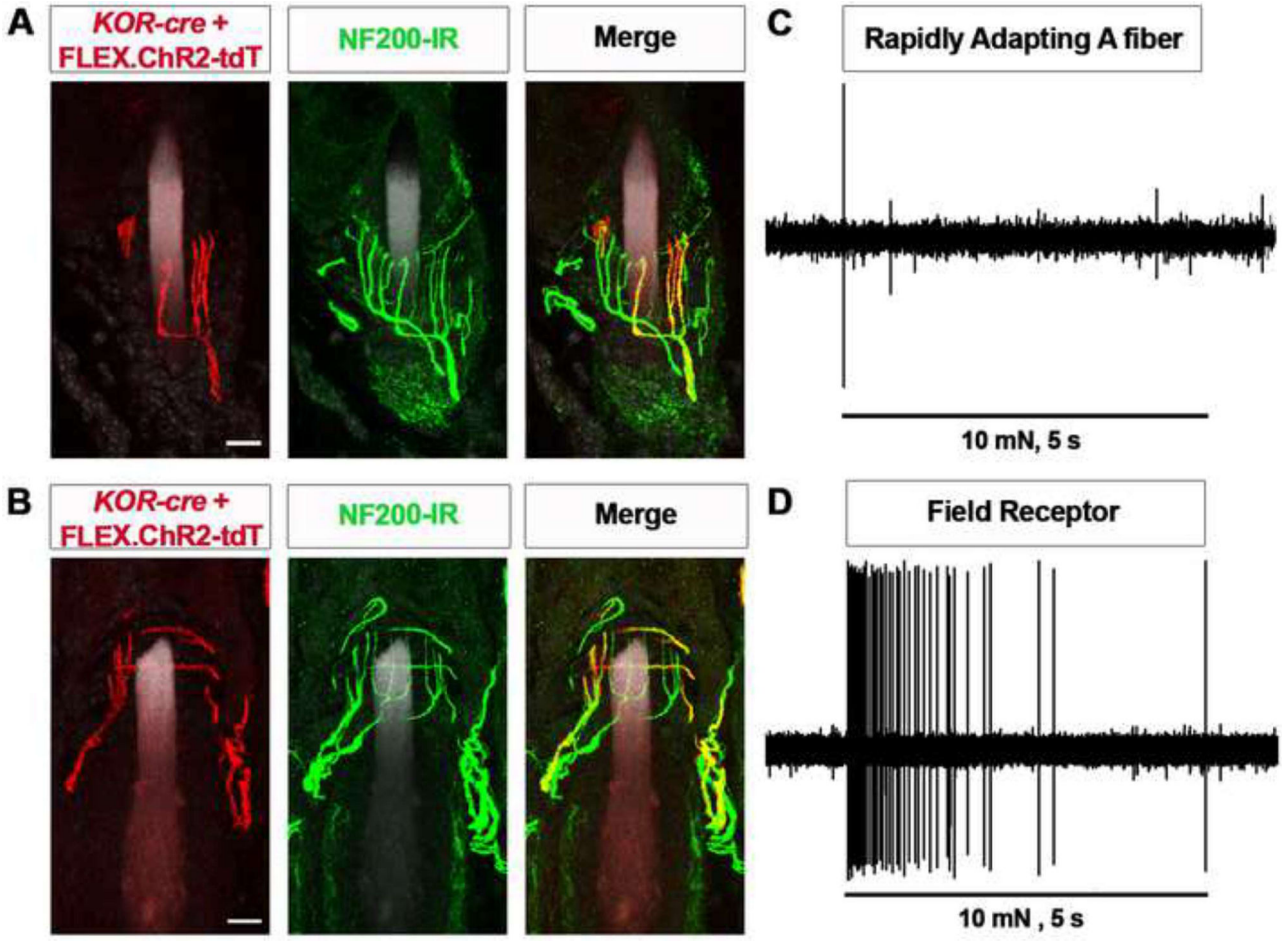

Figure 3. *KOR-cre* mediates recombination of lanceolate afferents and circumferential field receptors

A - B. IHC illustrating examples of a *KOR-cre*-labeled (red) lanceolate fiber (A) or circumferential fiber (B) innervating hair follicles in the hindpaw skin and co-localization with NF200 (green). *KOR-cre* afferents were labeled with a Cre-dependent virus (AAV.FLEX.ChR2-tdTomato; IT in adult). Data are representative of n = 2 mice. Scale bar = 10 μm.

C - D. Single fiber recordings were performed in *KOR-cre, ROSA*$^{lslChR2\text{-}eYFP}$ mice and fibers were identified with optogenetic tagging by their response to blue light stimulation of their cutaneous receptive field. A representative trace of a single fiber recording from a *KOR-cre*-positive rapidly adapting A-fiber (C) and large dynamic range fiber (D) upon application of a mechanical stimulus the receptive field in the skin (5 sec, 10 mN) Data are representative of n = 4 cells of each type.

Author Manuscript Author Manuscript Author Manuscript Author Manuscript

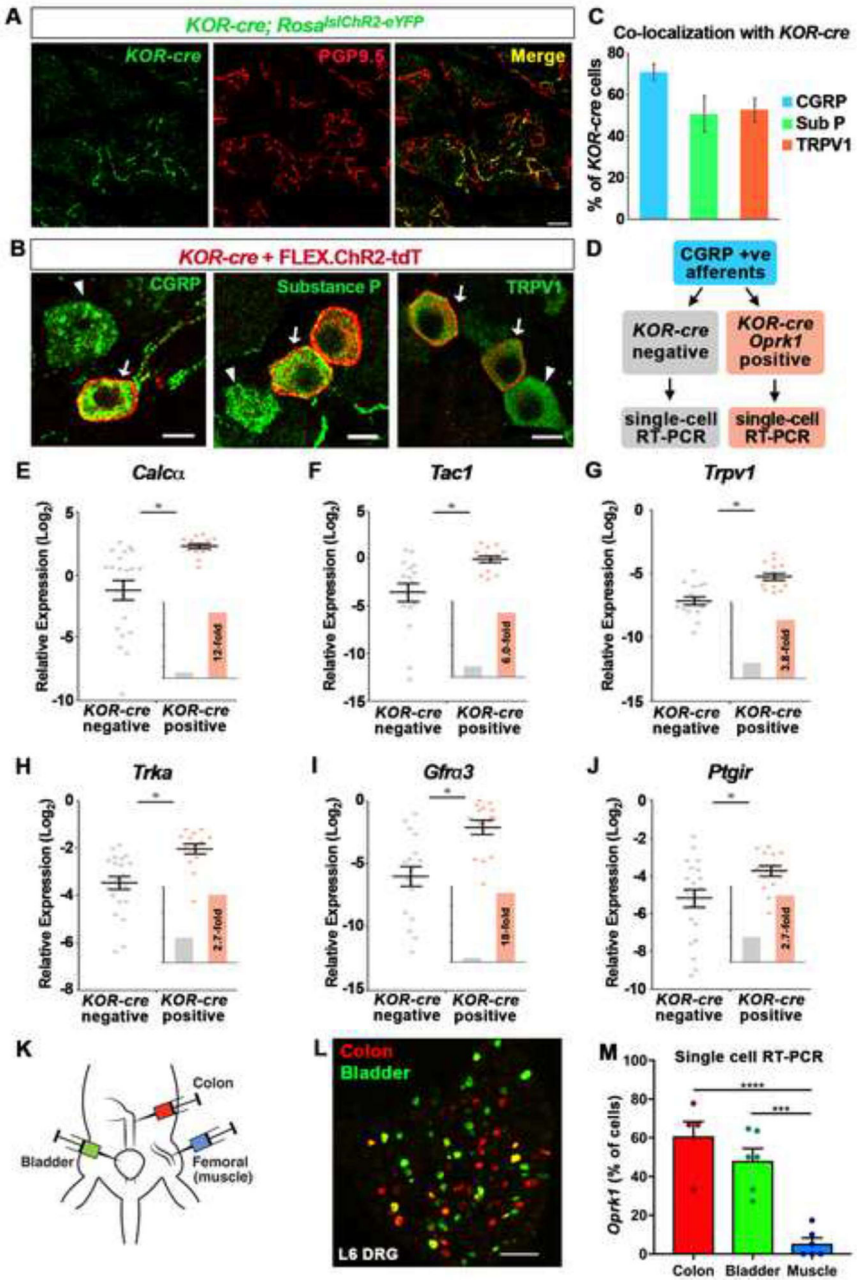

Figure 4. KOR is expressed by a transcriptionally distinct subset of peptidergic DRG neurons that preferentially target viscera.

A. Wholemount IHC of the thoracic skin from a *KOR-cre; Rosa*$^{lslChR2\text{-}eYFP}$ mouse showing that *KOR-cre*-positive afferents (green) make up a subset of free nerve endings that terminate in the epidermis, as assessed by co-localization with PGP9.5 (red). Scale bar = 10 μm.

B. IHC of DRG showing *KOR-cre*-labeled neurons co-localize with markers of peptidergic neurons. *KOR-cre* afferents were labeled with a Cre-dependent virus (AAV.FLEX.ChR2-tdTomato; IT in adult) Arrows indicate co-localization; arrowheads indicate CGRP-,

Author Manuscript Author Manuscript Author Manuscript Author Manuscript

Substance P- (SP), or TRPV1-expressing neurons that are not *KOR-cre* positive. Scale bar = 10 μm.

C. Quantification of (B) showing the percentage of *KOR-cre* + FLEX.ChR2-tdT cells that co-localize with peptidergic markers. Data are presented as mean ± SEM (n = 3 mice).

D. Schematic of single-cell RT-PCR experimental design. Lumbar DRG neurons from *KOR-cre; Rosa*$^{lslChR2\text{-}eYFP}$ mice were collected individually. Only peptidergic cells that expressed *Calca* were analyzed. Transcript levels were compared between *KOR-cre*-labeled neurons that showed clear *Oprk1* expression and *KOR-cre* negative neurons.

E - J. Expression levels of *Calca* (E), *Tac1* (F), *Trpv1* (G) *TrkA*, (H), *Gfra3* (I) and *Ptgir* (J) mRNA relative to *GAPDH* in *KOR-cre* negative (gray) and *KOR-cre* positive (orange) DRG neurons. Data are presented as the $-\log_2 \Delta CT$ expression relative to *GAPDH* expression within the same cell such that larger numbers represent higher mRNA expression. There was a significantly higher relative expression level of each transcript in *KOR-cre* positive neurons compared to *KOR-cre* negative neurons (Student's t-test, $p < 0.05$). Inset shows fold-increase in the average expression level normalized to the average expression in *KOR-cre* negative neurons. Black bars represent mean ± SEM and colored dots represent values from individual cells (n = 20 *KOR-cre* negative neurons, n = 15 *KOR-cre* positive neurons).

K. Cartoon illustrating the back-labeling of bladder, colon and muscle primary afferents using fluorophore-conjugated cholera toxin B and/or wheat germ agglutinin.

L. Image of L6 DRG in which colon afferents have been back-labeled with CTB-555 (red) and bladder afferents have been back-labeled with CTB-488 (green). Note, a small fraction of afferents dually innervate colon and bladder (yellow).

M. Analysis of *Oprk1* expression by single cell RT-PCR in afferents that innervate bladder, colon, or muscle. The proportion of bladder afferents or colon afferents that express *Oprk1* was significantly higher than the proportion of muscle afferents that express *Oprk1.* Data are presented as mean ± SEM and symbols represent data points from individual animals (*** < 0.001, **** < 0.0001, One-way ANOVA followed by Holm-Sidak test; n = 5 – 6 mice/condition with 9 – 22 cells per mouse).

Author Manuscript Author Manuscript Author Manuscript Author Manuscript

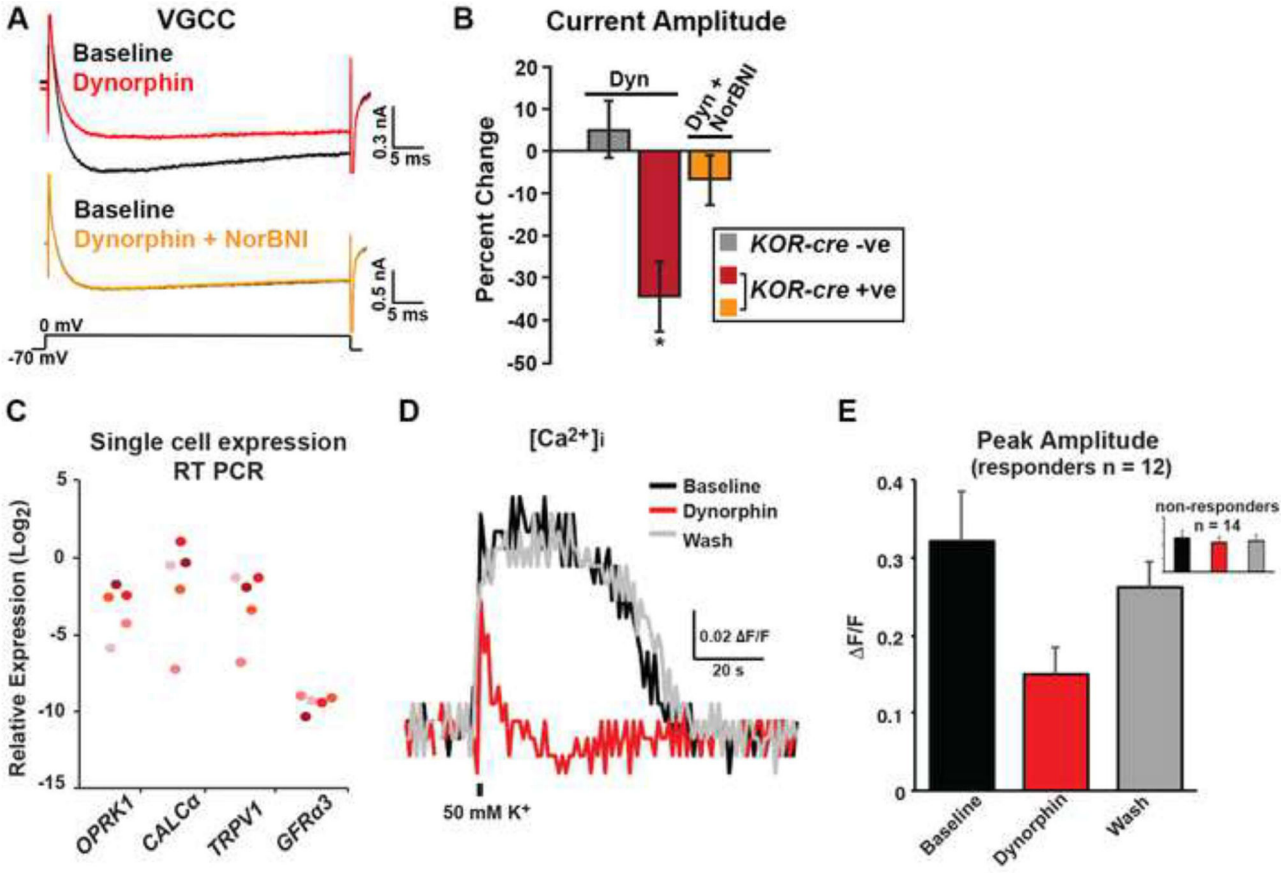

Figure 5. Activation of KOR inhibits voltage-gated Ca^{2+} currents in mouse DRG neurons and Ca^{2+} influx in human peptidergic DRG neurons.

A. Representative traces of voltage-gated Ca^{2+} currents (VGCC) in a genetically-labeled cell from a *KOR-cre; Rosa*$^{lsl\text{-}tdTomato}$ mouse at baseline (black traces, top and bottom), in the presence of dynorphin (1 μm, red; top trace), and in the presence of dynorphin (1 μm) + norBNI (1 μm, yellow; bottom trace). Neurons were held at −70 mV and a 50 ms step to 0 mV was applied.

B. Quantification of the percent change in current amplitude of *KOR-cre* negative neurons (gray; n = 5), *KOR-cre* positive neurons in the presence of dynorphin (1 μm; red; n = 6), or *KOR-cre* positive neurons in the presence of dynorphin (1 μm) + norBNI (1 μm; orange; n = 3). There was a significant decrease in current amplitude in the presence of dynorphin in *KOR-cre* positive neurons (*, paired t-test, $p < 0.05$). Data are presented as mean ± SEM.

C. Expression levels of *OPRK1*, *CALCα*, *TRPV1*, and *GFRα3* mRNA in human DRG neurons. Each neuron is represented by a different color. Data are presented as the $-\log_2$ ΔCT expression relative to *GAPDH* expression within the same cell such that larger numbers represent higher mRNA expression. All *OPRK1*-expressing cells expressed mRNA for the peptidergic markers *CALCα*, *TRPV1*, and *GFRα3.*

D - E. Representative traces (D) and quantification (E) of human DRG neuron Ca^{2+} responses to a brief (800 ms) application of high K^+ evoked (50 mM) before (black), during (red) and after (gray) the application of dynorphin (1 μM). The response to dynorphin was

Author Manuscript Author Manuscript Author Manuscript Author Manuscript

significant (greater than 2 standard deviations of the baseline response) in 12 of 26 neurons from 4 donors. Inset shows 14 non-responders. Data are presented as mean ± SEM.

Author Manuscript Author Manuscript Author Manuscript Author Manuscript

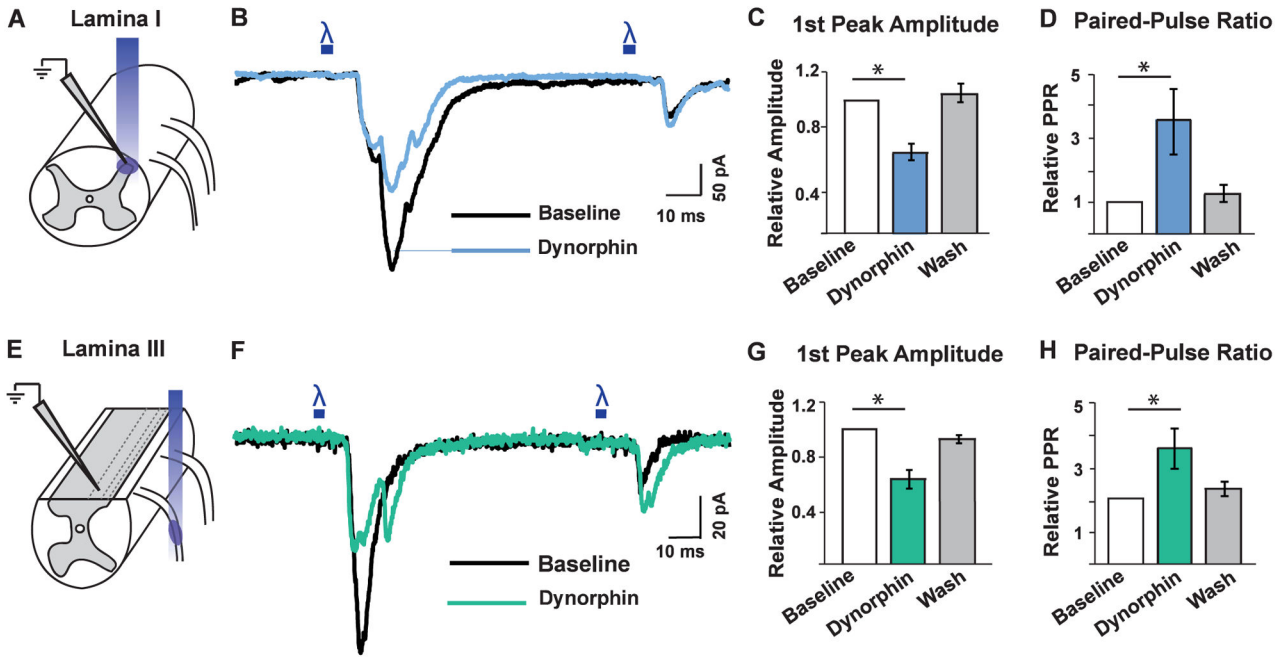

Figure 6. KOR activation reduces excitatory neurotransmission from primary afferents that target lamina I and lamina III.

A. Schematic illustrating the experimental set-up used to record from lamina I dorsal horn neurons while optogenetically stimulating KOR-cre primary afferent terminals. *KOR-cre* primary afferents were infected with a Cre-dependent virus encoding ChR2 (AAV.FLEX.ChR2-tdTomato; IP, P1) enabling selective activation of *KOR-cre* primary afferent terminals upon application of blue light to the spinal cord.

B. Representative trace of whole-cell patch clamp recording from a lamina I neuron at baseline (black) and during bath application of dynorphin (1 μM; blue). Two 5 ms pulses of blue light were given 100 ms apart to elicit light-evoked EPSCs.

C - D. Quantification of the amplitude of the first eEPSC (D) and paired-pulse ratio (D) at baseline (white), upon application of dynorphin (1 μM; blue), and following wash (gray). Dynorphin caused a significant decrease in the amplitude of the first eEPSC compared to baseline in lamina I neurons and a significant increase in the paired-pulse ratio compared to baseline, which was reversible (One-way ANOVA and Dunnett's multiple comparison's test, $p < 0.05$; $n = 14$ cells). Data are presented as mean ± SEM. There was no significant change in the 2nd peak amplitude during dynorphin application compared to baseline ($p = 0.1$; data not shown)

E. Schematic illustrating the experimental set-up used to record from lamina III dorsal horn neurons while optogenetically activating *KOR-cre* primary afferents. *KOR-cre, ROSA$^{lslChR2\text{-}eYFP}$* mice were used for these experiments and thus blue light stimulation was applied to the dorsal root in order to selectively activate *KOR-cre* primary afferents and not KOR-expressing spinal neurons.

F. Representative trace of whole-cell patch clamp recording from a lamina III neuron at baseline (black) and during bath application of dynorphin (1 μM; green). Two 5 ms pulses of blue light were given 100 ms apart to elicit light-evoked EPSCs.

Author Manuscript Author Manuscript Author Manuscript Author Manuscript

G - H. Quantification of the first eEPSC relative amplitude (G) and paired pulse ratio (H) at baseline (white), upon application of dynorphin (1 μM; green), and following wash (gray). Dynorphin caused a significant decrease in the amplitude of the first eEPSC and a significant increase in the paired-pulse ratio compared to baseline in lamina III neurons, which was reversible (One-way ANOVA, Dunnett's multiple comparison's test, $p < 0.05$; $n = 6$ cells). Data are presented as mean ± SEM. There was no significant change in the 2nd peak amplitude during dynorphin application compared to baseline ($p = 0.8$, data not shown).

Author Manuscript Author Manuscript Author Manuscript Author Manuscript

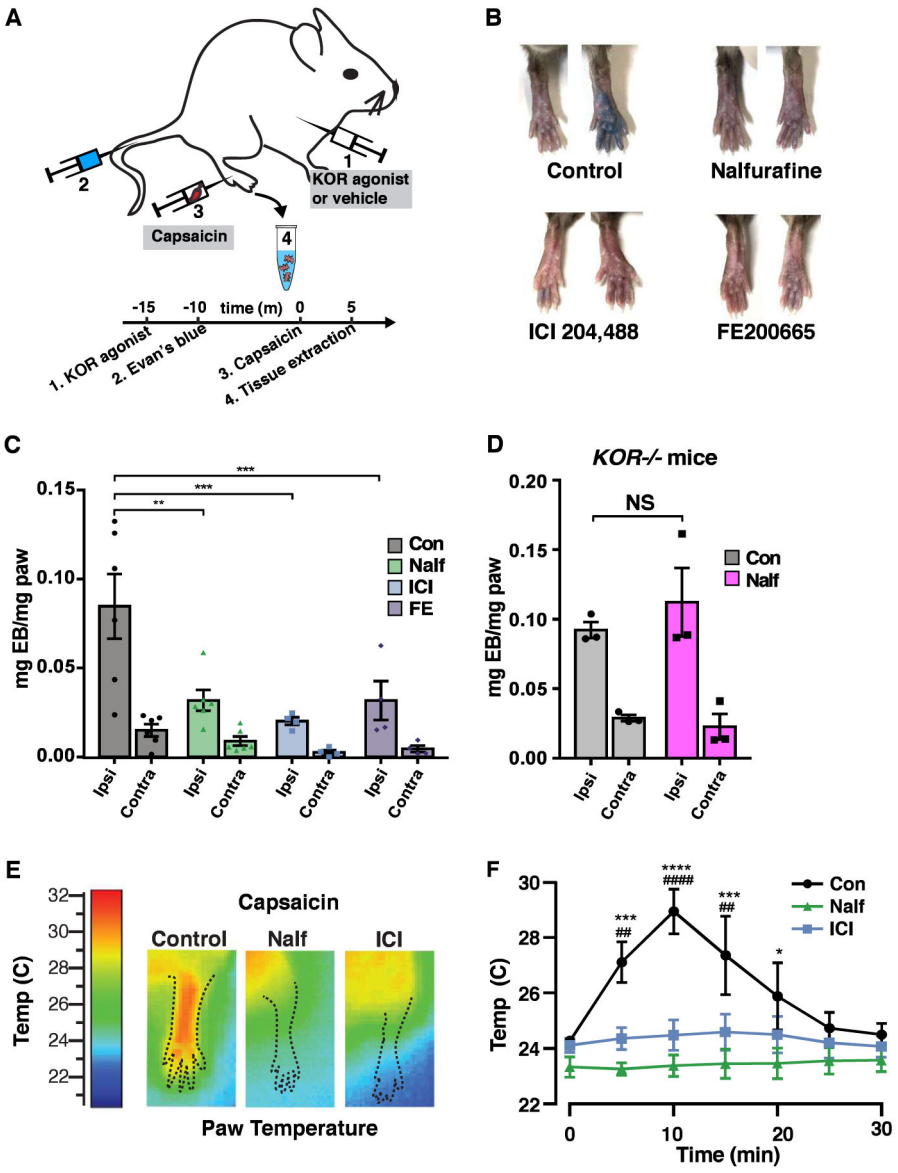

Figure 7. Peripherally restricted KOR agonists inhibit neurogenic inflammation

A. Schematic illustrating experimental design to measure the effect of KOR agonists on plasma extravasation induced by capsaicin.

B - C. Representative images (B) and quantification (C) of Evans blue extravasation upon injection of capsaicin (0.1%) into the ipsilateral paw of mice pretreated with vehicle (Control), nalfurafine (20 μg/kg), ICI204,448 (10 mg/kg) or FE200665 (12 mg/kg), as indicated. Data are presented as mean ± SEM and symbols represent data points from individual animals (two-way ANOVA, Tukey's post hoc test; * $p < 0.05$; n = 4 – 6 mice/condition).

D. Capsaicin-induced Evans blue extravasation in *KOR−/−* mice treated with vehicle (Con) or nalfurafine (Nalf, 20 μg/kg). Data are represented as mean + SEM and symbols represent data points from individual animals (two-way ANOVA; NS $p > 0.05$; n = 3 mice/condition)

Author Manuscript Author Manuscript Author Manuscript Author Manuscript

E - F. Representative images (F) and quantification (G) of infrared thermography to assess paw temperature. Injection of capsaicin (0.1%) caused a transient increase in the temperature of the ipsilateral paw of mice pretreated with vehicle (Control), which was significantly greater than that observe in mice pretreated with nalfurafine (20 μg/kg) or ICI204,448 (10 mg/kg), as indicated. Data represent mean ± SEM (two-way ANOVA followed by Holm-Sidak multiple comparison test; * or # indicates $p < 0.05$ between nalfurafine and vehicle or ICI and vehicle groups, respectively; $n = 4 – 5$ mice/condition).

Author Manuscript Author Manuscript Author Manuscript Author Manuscript

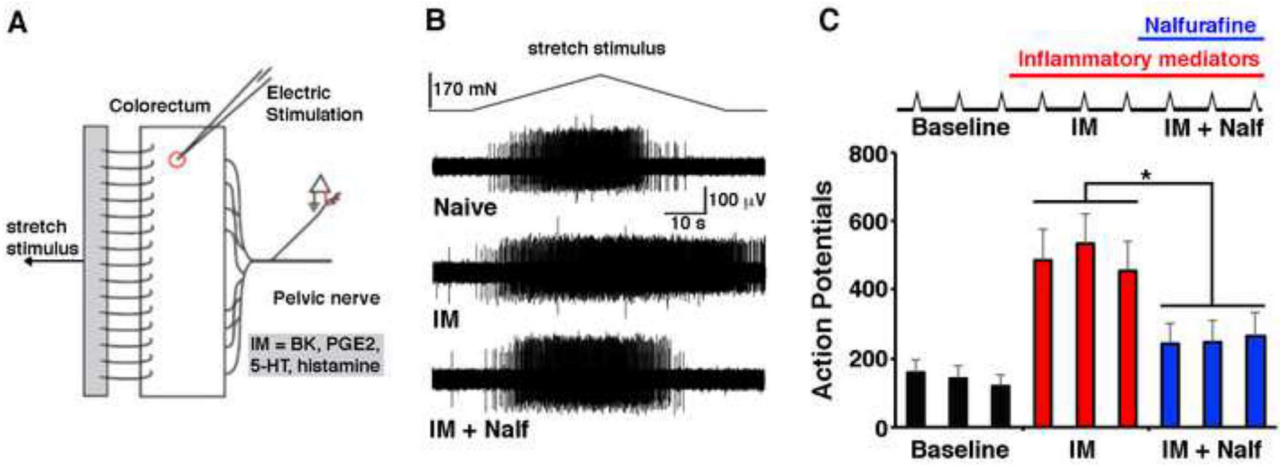

Figure 8. KOR signaling in the periphery inhibits inflammatory mediator-induced sensitization of nociceptive afferents

A. Schematic of the colon-nerve preparation and isolation of the receptive field.

B. - C. Typical recording (B) and quantification (C) of a teased fiber response to stretch (top trace) before (baseline) and after application of inflammatory mediators (IM: histamine, bradykinin, prostaglandin E2, and serotonin, each at 10 μM) or the combination of inflammatory mediators and 10 nM nalfurafine (IM + Nalf). Data represent mean + SEM (One-way RM AVOVA, Holm-Sidak post hoc; * $p < 0.05$; $n = 8$ afferents from 8 mice).

Author Manuscript Author Manuscript Author Manuscript Author Manuscript

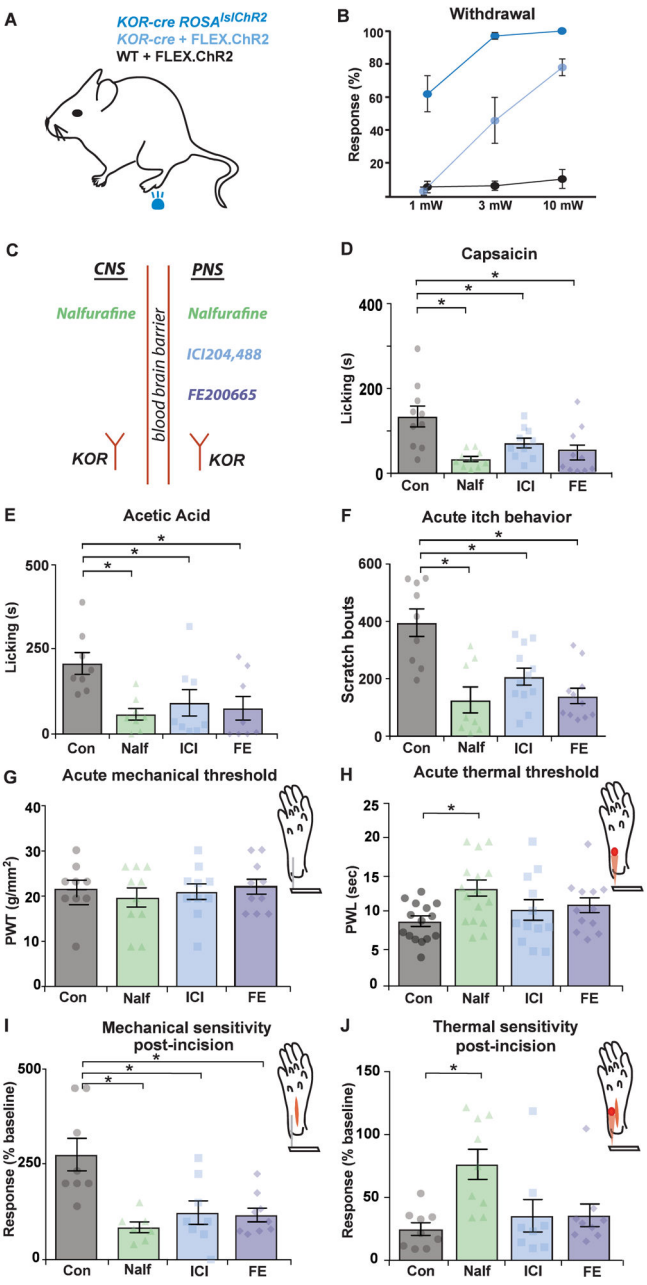

Figure 9. Peripherally restricted KOR agonists inhibit chemical pain, itch, and mechanical hypersensitivity following incision.

A. Schematic of optogenetic withdrawal experimental design. Blue light (470 nm) LED stimulation was applied to the glabrous hindpaw for 1 s. Three different groups were tested; *KOR-cre; ROSA*^{lslChR2} mice, *KOR-cre* mice + FLEX.ChR2 (IP at P1), and the wild-type littermates (WT) + FLEX.ChR2 (IP at P1).

B. The frequency withdrawal upon optogenetic stimulation at three different LED intensities (1 mW, 3 mW, and 10 mW). Data are presented as mean ± SEM (n = 4 – 6 mice/group with 10 stimulus presentations per mouse).

Author Manuscript Author Manuscript Author Manuscript Author Manuscript

C. Schematic diagram illustrating KOR agonists used in behavioral assays in D - J. Nalfurafine acts both centrally and peripherally, whereas ICI204,488 and FE200665 are peripherally restricted KOR agonists. Nalfurafine (Nalf; 20 μg/kg), ICI204,448 (ICI; 10 mg/kg), and FE200665 (FE; 12 mg/kg) were given IP 15 minutes prior to behavioral testing. All data are presented as mean ± SEM and colored symbols represent data points from individual animals.

D. Capsaicin-induced licking behavior (20 μL, intraplantar, 1.5%) was significantly reduced by Nalf, ICI, or FE (One-way ANOVA with Dunnett's multiple comparison's test, $p < 0.001$; $n = 10$ mice/group).

E. Acetic acid-induced licking behavior (20 μL intraplantar, 0.6%) was significantly reduced by Nalf, ICI, or FE (One-way ANOVA, Dunnett's multiple comparison's test, $p < 0.05$; $n = 10$ mice/group).

F. Chloroquine-induced scratching behavior (20 μL intradermal, 200 μg) was significantly reduced by Nalf, ICI, or FE (One-way ANOVA with Dunnett's multiple comparison's test, $p < 0.001$; $n = 8 – 12$ mice/group).

G. Paw withdrawal threshold (PWT) as measured by the von Frey test was not significantly changed by Nalf, ICI, or FE (One-way ANOVA, $p = 0.8$; $n = 9 – 10$ mice/group).

H. Nalfurafine significantly increased paw withdrawal latency (PWL) as measured by the Hargreaves' test, but ICI and FE had no effect on PWL (One-way ANOVA with Dunnett's multiple comparison's test (* $p < 0.05$; $n = 12 – 16$ mice/group).

I. Mechanical hypersensitivity, measured 2 hours after an incision of the hindpaw, was significantly reduced by Nalf, ICI, or FE (One-way ANOVA, Dunnett's multiple comparison's test, $p < 0.001$; $n = 7 – 9$ mice/group). Mechanical sensitivity was recorded as the number of withdrawal responses (out of 10) to a single von Frey fiber (vF # 3.61, 0.4g) applied to the plantar surface of the paw adjacent to the incision. Data are normalized to a baseline measure recorded 24 hours prior to the incision.

J. Thermal hypersensitivity, measured 2 hours after an incision of the hindpaw, was significantly reduced by Nalf (One-way ANOVA with Dunnett's multiple comparison's test, *, $p < 0.01$), whereas ICI or FE had no significant effect ($p > 0.05$; $n = 8 – 9$ mice/group). Data are normalized to a baseline measure recorded 24 hours prior to the incision.

Author Manuscript Author Manuscript Author Manuscript Author Manuscript

KEY RESOURCES TABLE

REAGENT or RESOURCE	SOURCE	IDENTIFIER
Antibodies		
Sheep anti-CGRP	Abcam	Cat# ab22560
Rabbit anti-NF200	Sigma Aldrich	Cat# N4142
Mouse anti-NF200	Sigma Aldrich	Cat# N0142
Rabbit anti-TH	Millipore	Cat# AB152
Mouse anti-Parvalbumin	Millipore	Cat# MAB1572
Rabbit anti-PGP9.5	UltraClone Limited	Cat# RA95101
Goat anti-TRPV1	Santa Cruz Biotechnology	Cat# sc-12489
Rabbit anti-Substance P	ImmunoStar	Cat# 20064
Rabbit anti-RFP	Rockland Antibodies & Assays	Cat# 600-401-379S
Rabbit anti-Trpm8	gift from M.Tominga, Okazai Institute for Integrative Bioscience	
Bacterial and Virus Strains		
AAV9.CAGGS.FLEX.ChR2-tdtomato.WRPE.SV40	Penn Vector Core	Addgene18917
Chemicals, Peptides, and Recombinant Proteins		
Isolectin B4 (BSI-B4), biotin conjugate	Sigma Aldrich	Cat# L2140
Dynorphin A	Tocris Biosciences	Cat# 3195
nor-Binaltorphimine dihydrochloride	Tocris Biosciences	Cat# 0347
ICI204,488 hydrochloride	Tocris Biosciences	Cat# 0822
Naloxone hydrochloride	Tocris Biosciences	Cat# 0599
Nalfurafine	Adooq Bioscience	Cat# A12579
FE200665	from F. Porreca, University of Arizona	
RNAscope Probe- Mm-Oprk1	Advanced Cell Diagnostics	Cat# 316111
RNAscope Probe- tdTomato-C2	Advanced Cell Diagnostics	Cat# 317041-c2
Critical Commercial Assays		
RNAscope Multiplex Fluorescent Assay	Advanced Cell Diagnostics	Cat# 320850
MessageBOOSTER cDNA Sythesis Kit from Cell Lysates Kit	Epicentre	Cat# MBCL90310
RNA Clean & Concentrator-5	Zymo Research	Cat# R1015

Author Manuscript Author Manuscript Author Manuscript Author Manuscript

REAGENT or RESOURCE	SOURCE	IDENTIFIER
SsoAdvanced Universal SYBR Green Supermix	BioRad	Cat# 1725270
RNAscope Multiplex Fluorescent Assay	Advanced Cell Diagnostics	Cat# 320850
Experimental Models: Organisms/Strains		
Mouse: wild type C57BL/6	Charles River	Strain Code 027
Mouse: *KOR-cre*	Cai et al., 2016	
Mouse: Ai9 *Rosa26-LSL-tdTomato*	The Jackson Laboratory	Stock No 007905
Mouse: Ai32 *Rosa26-LSL-ChR2/EYFP*	The Jackson Laboratory	Stock No 024109
Other		
Nikon Elements Advanted Research	Nikon	https://www.nikoninstruments.com/Products/Software/NIS-Elements-Advanced-Research
R	The R Project for Statistical Computing	https://www.r-project.org/
GraphPad Prism 7	GraphPad Software	https://www.graphpad.com/scientific-software/prism/
pClamp 10	Molecular Devices	https://www.moleculardevices.com/systems/conventional-patch-clamp/pclamp-10-software
Clampfit	Molecular Devices	https://www.moleculardevices.com/systems/conventional-patch-clamp/pclamp-10-software
Signal 6	Cambridge Electronic Design	http://ced.co.uk/products/sigovin
Spike 2	Cambridge Electronic Design	http://ced.co.uk/products/spkovin
Excel	Microsoft	https://products.office.com/en-us/excel
Illustrator CS5.1	Adobe	https://www.adobe.com/creativecloud.html?promoid=KLXLR
Photoshop CS5.1	Adobe	https://www.adobe.com/creativecloud.html?promoid=KLXLR